



## RESEARCH ARTICLE

10.1029/2024JD043110

### Key Points:

- We simulate aromatics in South Korea with the GEOS-Chem chemical transport model and improve model biases for benzene and phenol
- Our results suggest toluene and ethylbenzene are atmospherically relevant precursors of phenol
- Benzaldehyde is found to be the dominant source of nitrophenol in the model

### Supporting Information:

Supporting Information may be found in the online version of this article.

### Correspondence to:

S. M. MacFarlane,  
smm997@uowmail.edu.au







### Citation:

MacFarlane, S. M., Fisher, J. A., Xu, L., Wennberg, P. O., Crounse, J. D., Ball, K., et al. (2025). Sources, sinks, and oxidation pathways of phenolic compounds in South Korea constrained using KORUS-AQ airborne observations. *Journal of Geophysical Research: Atmospheres*, 130, e2024JD043110. <https://doi.org/10.1029/2024JD043110>

Received 4 DEC 2024

Accepted 13 JUN 2025

# Sources, Sinks, and Oxidation Pathways of Phenolic Compounds in South Korea Constrained Using KORUS-AQ Airborne Observations

Stephen M. MacFarlane<sup>1</sup> , Jenny A. Fisher<sup>1,2</sup> , Lu Xu<sup>3</sup>, Paul O. Wennberg<sup>4</sup> , John D. Crounse<sup>4</sup> , Katherine Ball<sup>4</sup>, Shixian Zhai<sup>5</sup>, Kelvin H. Bates<sup>6</sup>, Younha Kim<sup>7</sup>, Qiang Zhang<sup>8</sup> , and Donald R. Blake<sup>9</sup> 

<sup>1</sup>Environmental Futures, University of Wollongong, Wollongong, NSW, Australia, <sup>2</sup>College of Science and Engineering, James Cook University, Douglas, QLD, Australia, <sup>3</sup>Department of Energy, Environmental and Chemical Engineering, Washington University in St. Louis, St. Louis, MO, USA, <sup>4</sup>California Institute of Technology, Pasadena, CA, USA, <sup>5</sup>Department of Earth and Environmental Sciences, Faculty of Science, The Chinese University of Hong Kong, Hong Kong, China, <sup>6</sup>Department of Mechanical Engineering, University of Colorado Boulder, Boulder, CO, USA, <sup>7</sup>International Institute for Applied Systems Analysis (IIASA), Laxenburg, Austria, <sup>8</sup>Tsinghua Center for Green Chemical Engineering Electrification (CCEE), Beijing Key Laboratory of Green Chemical Reaction Engineering and Technology, Department of Chemical Engineering, Tsinghua University, Beijing, China, <sup>9</sup>Department of Chemistry, University of California Irvine, Irvine, CA, USA

**Abstract** Aromatics are an important class of volatile organic compounds with impacts on human health. The impacts of aromatics and their oxidation products vary. While the chemistry and major pathways of the precursor aromatics are relatively well understood, the same is not true for their phenolic oxidation products. Here, we use new observations of aromatic oxidation products collected during the Korea-United States Air Quality aircraft campaign to evaluate the aromatic chemical mechanism in the GEOS-Chem v13.4.0 chemical transport model. Based on these results, we implement changes to emissions, add ethylbenzene chemistry, and introduce phenol production from ethylbenzene and toluene oxidation. These changes improve simulation of benzene (reducing normalized mean bias from 24% to −9%) and phenol (−71% to −42%). Model biases increase for toluene, xylene, and cresol, but simulated mixing ratios remain within measurement uncertainties and observed interquartile ranges. We identify potential toluene emission overestimates from petrochemical complexes in Ulsan and Daesan and underestimates from the Daegu dyeing industrial complex, and underestimates of benzene emissions from China. Using the updated model, we find benzene and toluene contribute equally to phenol production in the boundary layer (accounting for 40% of phenol production each), and that toluene and ethylbenzene are atmospherically relevant precursors of phenol. Phenol and cresol loss is found to be dominated by OH oxidation (73% for both phenol and cresol). We find that benzaldehyde is the dominant source of nitrophenol production (67%), although phenol dominates nitrophenol production at night.

**Plain Language Summary** Aromatics are a group of trace gases emitted by human activities that have negative impacts on air quality and public health. The impacts vary depending on the chemistry, which can follow various pathways and form different products. To better understand the impacts of aromatics in the atmosphere, this study uses a model of the South Korean atmosphere to investigate the major chemical pathways of three aromatic compounds: phenol, cresol, and nitrophenol. The model was evaluated using aircraft measurements from South Korea, then updated to improve accuracy. Adding a new chemical pathway to form phenol for two other aromatics (toluene and ethylbenzene) improved the model's accuracy, suggesting these may be important phenol sources—a result that had previously only been identified in laboratory experiments. The major loss pathway of phenol and cresol was found to be a reaction pathway that is expected to lead to more particulate matter production. However, in urban environments with high population, the major loss pathway was instead one that produces nitrophenols, which are highly toxic.

## 1. Introduction

Aromatics are an important subset of volatile organic compounds (VOCs) that have significant impacts on human health (Kroflíč et al., 2015; Rajabi et al., 2020; Tiwari et al., 2019) and contribute to both ozone and secondary organic aerosol (SOA) formation (Seinfeld & Pandis, 2016). The nature of their impacts on air quality and human

© 2025 The Author(s).

This is an open access article under the terms of the [Creative Commons Attribution-NonCommercial License](#), which permits use, distribution and reproduction in any medium, provided the original work is properly cited and is not used for commercial purposes.

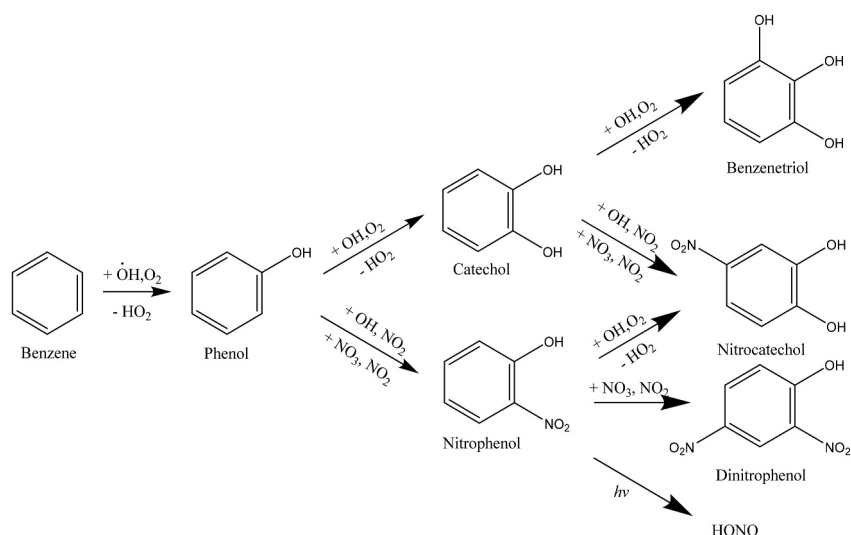


**Figure 1.** A simplified representation of the aromaticity-retaining benzene oxidation cascade.

health are linked to their oxidation chemistry, with different impacts depending on the reaction pathway followed. While the reaction kinetics and major loss pathways of the precursor aromatics (benzene, toluene, ethylbenzene, and xylene, referred to collectively as BTEX) are well understood, the major loss pathways of their oxidation products, including phenol, cresol, and nitrophenols, are relatively unknown. These oxidation products have previously been included in model chemical mechanisms (Bates et al., 2021; Emmons et al., 2020; Yan et al., 2019), but no measurements were available for validation. Here, we use new measurements of aromatic oxidation products (phenol, cresol, and nitrophenols) observed during the Korea-United States Air Quality study (KORUS-AQ) to evaluate and improve the representation of the aromatic oxidation cascade in a 3D chemical transport model (GEOS-Chem). From there, we use the improved model to quantify the budget of first-generation oxidation products in the South Korean region.

Aromatics are emitted primarily by anthropogenic sources, including vehicle exhaust, fossil fuel consumption, and solvent usage, with additional emissions from biofuel and biomass burning (Cabrera-Perez et al., 2016; Koppmann, 2007; Zeng et al., 2019). Aromatics can account for up to 60% of tropospheric VOCs over urban and semi-urban areas, with the most abundant being the BTEX species (Cabrera-Perez et al., 2016; Yan et al., 2019). Once in the atmosphere, aromatic compounds undergo multiple steps of oxidation, yielding a variety of species including phenols, catechols, aldehydes, nitrophenols, glyoxal, and formic acid. This chemistry can enhance both ozone and SOA production (Bates et al., 2021) or produce compounds with high toxicity, with the specific impacts dependent on which chemical pathways are followed and which species are produced as a result. For example, the reaction of phenol with OH radicals produces catechol, which has low vapor pressure resulting in high SOA yields when further oxidized (Finewax et al., 2018; Fredrickson et al., 2022), whereas reaction with nitrate ( $\text{NO}_3$ ) produces nitrophenol, which results in less SOA upon further oxidation (Bejan et al., 2020).

A simplified aromaticity-retaining reaction pathway for aromatic oxidation is shown in Figure 1, using benzene as an example. While a secondary major loss pathway for BTEX reaction with OH is the bicyclic peroxy radical pathway (up to 47% for benzene), which produces ring-breaking products such as glyoxal and butenedial (Wang et al., 2013), our focus here is on the ring-retaining phenolic pathways. The first stage of the atmospheric oxidation cascade, oxidation of the precursor aromatic (BTEX species), is relatively well understood. The major loss pathway of BTEX species is reaction with OH (Cabrera-Perez et al., 2016) to form a phenolic species (Baltaretu et al., 2009; Fan & Zhang, 2006; Wang et al., 2013). The subsequent oxidation chemistry is less well understood. Oxidation of first-generation products (e.g., phenolic species) follows one of two reaction pathways: either reaction with OH radicals, typically resulting in OH addition to the aromatic ring to form a catechol, or reaction with  $\text{NO}_3$  to produce nitroaromatics. Oxidation by OH can also initiate nitroaromatic formation by producing a phenoxy radical intermediate before reacting with  $\text{NO}_2$  to form the nitroaromatic, although the yield is typically much smaller than when the phenolic compound reacts with  $\text{NO}_3$ . The dominant loss pathways of phenolic species remain largely unexplored. Using a box model, Yuan et al. (2016) found that phenol was equally

likely to be removed via reaction with OH as with NO<sub>3</sub> in Utah, US in winter, but they did not explore other oxidation products, locations, or seasons. To date, limited measurements of aromatic oxidation products have been available to test our understanding of these oxidation pathways.

In this paper, we leverage new measurements of first-generation aromatic oxidation products (phenol, cresol, nitrophenol, nitrocresol, nitrocatechol, and nitromethylcatechol) to constrain their budgets in a region with high aromatic emissions (South Korea). We first evaluate and improve the representation of aromatic oxidation in the GEOS-Chem chemical transport model using airborne observations from KORUS-AQ. Our improvements include adjusted aromatic emissions ratios; additional emissions from volatile chemical products (Coggon et al., 2021; McDonald et al., 2018), biomass burning (Andreae, 2019; Finewax et al., 2018; Koss et al., 2018; Majdi et al., 2019), and car exhaust (Song et al., 2021); inclusion of ethylbenzene chemistry (Bates et al., 2021), and addition of phenol production from toluene and ethylbenzene (Birdsall & Elrod, 2011; Forstner et al., 1997; Noda et al., 2009). We then use the improved model to quantify the sources and atmospheric fates of phenol and cresol over South Korea.

## 2. Materials and Methods

### 2.1. KORUS-AQ Airborne Observations

The KORUS-AQ study was an airborne campaign that took place in May–June 2016 in South Korea, conducted jointly by the U.S. National Aeronautics and Space Administration (NASA) and the South Korea National Institute of Environmental Research (NIER) (Crawford et al., 2021). It featured three aircraft as well as ground-based sites and ships (Crawford et al., 2021). In this work, we exclusively use measurements from the DC-8 aircraft, including primary aromatics and their oxidation products. DC-8 flights were conducted on 23 days, typically reaching altitudes of up to ~12 km and sampling between Seoul and Jeju to the south, Busan to the southeast, Gangneung to the east, and the Yellow Sea to the west (Crawford et al., 2021). The KORUS-AQ flight track for altitudes below 2 km are shown in Figure 2a.

Whole air samples were collected onboard the DC-8, and from these, aromatic compounds including benzene, toluene, xylene, styrene, ethylbenzene, propylbenzene, ethyltoluene, and trimethylbenzene were measured using multi-column gas chromatography (Simpson et al., 2020). Here, we use 60-s merge data obtained from [https://www-air.larc.nasa.gov/cgi-bin/ArcView/korusaq?MERGE=1#60\\_SECOND.DC8\\_MRG/](https://www-air.larc.nasa.gov/cgi-bin/ArcView/korusaq?MERGE=1#60_SECOND.DC8_MRG/), with further averaging to match model resolution as described in Section 2.2.

We also use additional measurements for the aromatic oxidation products phenol, cresol, nitrophenol, nitrocresol, nitrocatechol, and nitromethylcatechol, which are not available in the merge files. These aromatic oxidation products were measured by the Caltech chemical ionization time-of-flight mass spectrometer using CF<sub>3</sub>O<sup>−</sup> as the reagent ion (Allen et al., 2022; Xu et al., 2020).

### 2.2. GEOS-Chem Model Description

We use GEOS-Chem version 13.4.0 (<https://doi.org/10.5281/zenodo.6511970>). The model is driven by Goddard Earth Observing System Forward-Processing (GEOS-FP) meteorological data from the NASA Global Modelling and Assimilation Office (GMAO). Baseline simulations were performed for May–June 2016 at two global resolutions (4° × 5° and 2° × 2.5°) and at a nested resolution (0.25° × 0.3125°) over East Asia with 72 vertical layers up to 0.01 hPa. The nested simulation used boundary conditions from the global simulation, with boundaries of 100–140°E and 20–50°N. Spin-up periods were 1 month for the global simulations and 2 weeks for the nested simulations, selected based on the short atmospheric lifetimes of the phenolic compounds of interest (a few hours to ~1 day). The in-built GEOS-Chem plane flight diagnostics were used to sample the GEOS-Chem output along the KORUS-AQ flight track at one-minute resolution. Both model output and observations were then averaged to obtain a single data point for each unique combination of model grid box and time step (20 min for global and 10 min for nested), with these averages used for all subsequent analysis.

#### 2.2.1. Emissions and Aromatic Oxidation Chemistry in the Baseline Simulation

Over Asia, the model was driven by anthropogenic emissions from the 2015 KORUSv5 emission inventory, except over China, where the year-specific Multi-resolution Emission Inventory for China (MEIC) were used (Zheng et al., 2018). The KORUSv5 emission inventory was developed at Konkuk University and is based on the

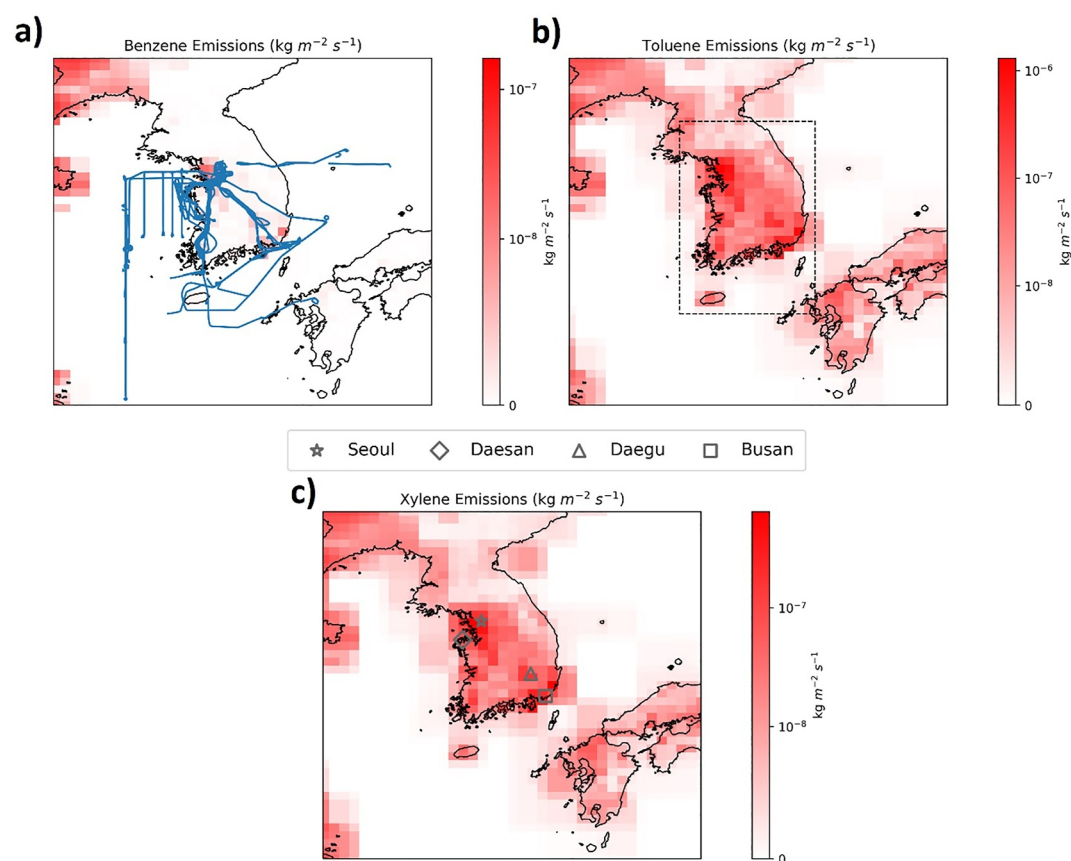


**Figure 2.** Aromatic emissions ( $\text{kg m}^{-2} \text{s}^{-1}$ ) in May–June 2015 from the updated simulation (see Section 2.2.2 for details) for (a) benzene, (b) toluene, and (c) xylene. Also shown are key geographic details referred to in the text: (a) KORUS-AQ flight path below 2 km, (b) the region used to calculate atmospheric budgets from the model (see Section 2.3 for details), and (c) key cities in South Korea.

CREATE inventory (Woo et al., 2020). The inventory includes emissions for carbon monoxide ( $\text{CO}$ ), ammonia ( $\text{NH}_3$ ),  $\text{NO}_x$ , fine particulate matter ( $\text{PM}_{2.5}$ ), sulfur dioxide ( $\text{SO}_2$ ), and VOCs including aromatics. VOC speciation in the original KORUSv5 inventory is based on the SAPRC-99 chemical mechanism, which includes two lumped aromatic species: ARO1 for less reactive aromatics such as benzene and toluene, and ARO2 for more reactive aromatics such as xylene (Carter, 1999). For use in GEOS-Chem, ARO1 was re-specified as 10% benzene and 90% toluene using scaling factors provided by S. Zhai, and ARO2 was assumed to be 100% xylene.

The MEIC emission inventory was developed by Tsinghua University and includes 10 species ( $\text{SO}_2$ ,  $\text{NO}_x$ ,  $\text{CO}$ , VOC,  $\text{NH}_3$ ,  $\text{PM}_{10}$ ,  $\text{PM}_{2.5}$ , black carbon, organic carbon, and carbon dioxide) from more than 700 anthropogenic sources in China (Zheng et al., 2018). The speciated emission inventory, including benzene, toluene, and xylene emissions was provided (Li et al., 2019). For MEIC, a sector-specific diurnal scaling factor was used following Miao et al. (2020).

For the global simulations, anthropogenic emissions outside of Asia were from the Community Emissions Data System (CEDSv2) emission inventory. Biogenic emissions were calculated online using the Model of Emissions of Gases and Aerosols from Nature (MEGANv2.1) (Guenther et al., 2012). Biomass burning emissions were from the Global Fire Emissions Database (GFEDv4.1s), including benzene, toluene, and xylene.

The GEOS-Chem simulation of aromatic oxidation chemistry is described in detail by Bates et al. (2021), and we use this as our baseline simulation. In brief, the mechanism includes 17 aromatic species including benzene, toluene, lumped xylenes, benzaldehyde, perbenzoic acid, peroxybenzoylnitrate, phenol, lumped cresols (cresol and xylenol), lumped catechols (catechol and methylcatechol), lumped nitroaromatics (nitrophenol, nitrocresol, nitrocatechol, and nitromethylcatechol), and several radical intermediates. There are 44 aromatic-specific

**Table 1**

*Biomass Burning Emission Factors (EFs) in Units of (kg Species Emitted) (kg Dry Matter Burnt)<sup>−1</sup> for Phenol and Catechol for Six Land Cover Types*

Land cover type	Phenol EF	Catechol EF
Savanna, grassland, and shrubland	$4.3 \times 10^{-4}$	$9.0 \times 10^{-4}$
Boreal forest	$7.5 \times 10^{-4}$	$9.0 \times 10^{-4}$
Temperate forest	$2.5 \times 10^{-4}$	$9.0 \times 10^{-4}$
Deforestation (tropical) and degradation	$2.3 \times 10^{-4}$	$9.0 \times 10^{-4}$
Peat	$4.7 \times 10^{-4}$	$9.2 \times 10^{-4}$
Agricultural waste	$8.9 \times 10^{-4}$	$4.8 \times 10^{-4}$

reactions, including reaction of benzene, toluene, and xylene with OH, reaction of oxidation products (benzaldehyde, phenol, cresol, catechols, nitroaromatics) with OH and NO<sub>3</sub>, and a phenoxy-phenylperoxy radical cycle.

## 2.2.2. Modified GEOS-Chem Aromatics Simulation

Following analysis of the results from the baseline simulations (see Section 3.1), we implemented several updates to better simulate aromatics in South Korea. First, we identified and added missing emission sources not included in the baseline simulation. The first of these is emissions from volatile chemical products (VCPs), such as adhesives, coatings, and cleaning agents. VCPs are an important source of VOCs, including aromatics (McDonald et al., 2018), but are not included in the anthropogenic emission

inventories described above. We added VCP emissions for toluene, xylene, and several alkane species following the implementation of Bates et al. (2022), with emissions scaled to global population density for 2015. The scaling factors used here were  $6.84 \times 10^{-15}$  kg s<sup>−1</sup> person<sup>−1</sup> for toluene and  $1.07 \times 10^{-14}$  kg s<sup>−1</sup> person<sup>−1</sup> for xylene (Coggon et al., 2021; McDonald et al., 2018).

Phenol is known to be emitted by the combustion of fossil fuels and has been detected in car exhaust (Perrone et al., 2014). However, the KORUSv5 inventory does not include phenol emissions from mobile sources, and the MEIC inventory does not include primary phenol emissions from any sources. We added mobile-source phenol emissions to both inventories using a phenol:CO emission ratio from car exhaust of 0.0004 (kg phenol) (kg CO)<sup>−1</sup> (Song et al., 2021).

Biomass burning is also a significant source of phenolic compounds, including phenol and catechol (Fang et al., 2024; Finewax et al., 2018; Gkatzelis et al., 2024; Xu et al., 2021). Neither species is included in the default implementation of the GFEDv4.1s biomass burning inventory in GEOS-Chem. We added phenol emissions from biomass burning using emission factors from Andreae (2019), applied to GFEDv4.1s dry matter burnt (Table 1). We also added emissions of catechols from biomass burning using emission factors from Majdi et al. (2019) for savanna, temperate forest, and agricultural waste fires and from Koss et al. (2018) for peat fires (Table 1). We did not find any estimates of catechol emission factors for boreal or tropical fires in the literature, and so applied the same emission factor as used for savanna and temperate forest fires to these land cover types.

Next, we made several updates to the chemical mechanism, starting with the chemical sources of phenol. While benzene is the dominant chemical source of phenol, with yields of up to 61.2% (Noda et al., 2009) (GEOS-Chem yield: 54%), there is experimental evidence for direct phenol production from toluene oxidation, with yields of 4.7%–5.4% (Birdsall & Elrod, 2011; Noda et al., 2009). We expect this source could be important in South Korea, as high concentrations of toluene were measured during KORUS-AQ (Crawford et al., 2020). We implemented this chemistry in GEOS-Chem with a 5.4% yield of phenol as a product of the toluene + OH reaction (Noda et al., 2009).

Ethylbenzene oxidation is also a known source of phenol (Huang et al., 2010). While ethylbenzene is not included in the default GEOS-Chem v13.4.0 configuration used for our baseline simulation, Bates et al. (2021) included it as part of an optional extended GEOS-Chem mechanism that was added to the default configuration in v14.5.0. We implemented this extended mechanism here (consistent with the implementation in v14.5.0 onwards) and modified it to include phenol from reaction of ethylbenzene with OH radicals. To the best of our knowledge, there are no published values for the gas-phase yield of phenol from ethylbenzene. Instead, we estimate the phenol yield based on coincident measurements of the particle-phase phenol yields from ethylbenzene and toluene, measured by Forstner et al. (1997). From these, we calculate the ratio of particle-phase phenol production from ethylbenzene to that from toluene and apply this ratio to the gas-phase phenol yield from toluene. The particle-phase ratio implies roughly 2.1 times more phenol is produced from ethylbenzene oxidation than from toluene, from which we derive a phenol yield from ethylbenzene oxidation of 11.4%.

The addition of ethylbenzene to the chemical mechanism also necessitated a revision to the aromatic emission speciation in the KORUSv5 inventory. In the baseline simulation, we assumed KORUSv5 ARO1 emissions were 10% benzene and 90% toluene (see Section 2.2). To account for the ethylbenzene component, we used 2016 emissions reported by the South Korea Ministry of Environment (available at: <https://icis.me.go.kr/prtr/main.do>)



to calculate the percentage distribution of benzene (0.9%), toluene (74.3%), and ethylbenzene (24.8%) and applied this distribution to KORUSv5 ARO1 emissions. However, when we ran the model with emissions calculated using this speciation, we found a benzene underestimate and an ethylbenzene overestimate in the model, relative to the airborne observations. We therefore further modified the speciation to better match the observations. To do this, we first multiplied the speciation for benzene (0.9%) and ethylbenzene (24.8%) by the ratio between the observed and modeled surface concentrations in the simulation using the updated speciation (i.e.,  $\text{benzene}_{\text{obs}}/\text{benzene}_{\text{mod}} \times 0.9\%$ ). We then attributed the remaining ARO1 to toluene. This resulted in a final KORUSv5 ARO1 speciation of 1.3% benzene, 12.1% ethylbenzene, and 86.6% toluene, with total simulated emissions during KORUS-AQ shown in Figure 2. Note there is uncertainty in this method as BTEX emissions outside South Korea may be partly responsible for the original model biases, resulting in an overcorrection of KORUSv5 emissions. Travis et al. (2024) use similar speciation, although with higher benzene emissions (7% benzene; 83% toluene; 10% ethylbenzene).

Finally, we updated the reaction rate for catechol with OH. The value used in the standard version of GEOS-Chem ( $2.0 \times 10^{-11} \text{ cm}^3 \text{ molecule}^{-1} \text{ s}^{-1}$ ) does not match the value reported in Bates et al. (2021) ( $1.5 \times 10^{-11} \text{ cm}^3 \text{ molecule}^{-1} \text{ s}^{-1}$ ), and both are an order of magnitude lower than previously published values (Cabrera-Perez et al., 2016; Mellouki et al., 2021). This rate discrepancy was included in GEOS-Chem to properly account for the lumping of catechols, methylcatechols, and their OH addition products into a single species; to facilitate direct model-measurement comparisons, we updated this rate to  $1.5 \times 10^{-10} \text{ cm}^3 \text{ molecule}^{-1} \text{ s}^{-1}$  to match published values. We found that this update decreased simulated catechols by 37% in surface air (Figure S1 in Supporting Information S1).

We considered a number of further modifications that we tested with sensitivity simulations but ultimately decided not to include in our final simulation. These included changes to reaction rates for production and loss of various species in the aromatic oxidation cascade; however, we found that either our results were insensitive to the changes, or (in cases where they were sensitive) there was no evidence in the literature to justify changes to the reaction rates. We also tested the impact of separating lumped species (catechols and nitroaromatics) and applying unique reaction rates to each individual species, using rates from Mellouki et al. (2021) for catechols and from Cabrera-Perez et al. (2016) for nitroaromatics. We found that this modification had negligible impact on our simulation but increased the computational cost, and so retained the lumped species and lumped reaction rates from Bates et al. (2021).

### 2.3. Atmospheric Budget Analysis

We used the output of our improved simulation to calculate atmospheric budgets for phenol and cresols in the boundary layer. We saved GEOS-Chem diagnostics at hourly resolutions for chemical production and loss, dry deposition, wet deposition, and emissions. Budget calculations were based on output between the surface and an average altitude of 2.15 km for box-edge latitudes 32.9°–39.0° and box-edge longitudes 125.5°–129.8° (see Figure 2b), averaged over all days in the 2-month simulation period (May–June 2016). We maintained the hourly resolution to analyze diel variability.

To distinguish between different chemical pathways, we separated the lumped phenoxy-phenylperoxy radical cycles for phenol, cresol, and benzaldehyde, as shown in Figures S2–S4 in Supporting Information S1. All radical cycles use the same product yields and reaction rates and produce the same lumped nitroaromatic species (NPHEN) when the phenoxy radical reacts with  $\text{NO}_2$ . We added dummy species to the mechanism to separately track phenol production from benzene, toluene, and ethylbenzene; cresol production from toluene and xylene; phenol and cresol loss from reaction with OH and  $\text{NO}_3$ ; and the production of the lumped nitroaromatic species from each of the individual phenoxy-phenylperoxy radical cycles (i.e., individual tracers for each cycle). Table S1 in Supporting Information S1 provides the relevant reactions, key products, and dummy species used for this analysis. Dummy species were set to zero after the spin-up period to track their accumulation during the 2-month science simulation.

We also used the model output to quantify the relative fractions of phenol loss that form catechol versus nitrophenol. We first calculated the total production of the two dummy species that track the phenol loss pathways (PHENOH, PHENNO3; see Table S1) in the model surface layer across the 2-month simulation, as well as dry deposition ( $L_{\text{DryDep\_Phen}}$ ), and wet deposition ( $L_{\text{WetDep\_Phen}}$ ), all in  $\text{kg (grid cell)}^{-1}$ . The total phenol

loss ( $L_{\text{Total}}$ ) over the 2-month period was calculated as the sum of the two rates ( $L_{\text{OH\_Phen}} = \text{PHENOH}$  and  $L_{\text{NO}_3\text{\_Phen}} = \text{PHENNO}_3$ ) and total deposition ( $L_{\text{DryDep\_Phen}} + L_{\text{WetDep\_Phen}}$ ), as shown in Equation 1:

$$L_{\text{Total\_Phen}} = L_{\text{OH\_Phen}} + L_{\text{NO}_3\text{\_Phen}} + L_{\text{DryDep\_Phen}} + L_{\text{WetDep\_Phen}} \quad (1)$$

The fraction of the phenol loss that produces catechol ( $F_{\text{CAT}}$ ) was then determined by multiplying  $L_{\text{OH\_Phen}}$  by the yield of catechol from the phenol + OH reaction (0.8) and dividing the result by  $L_{\text{Total\_Phen}}$ , as shown in Equation 2:

$$F_{\text{CAT}} = (L_{\text{OH\_Phen}} \times 0.8) / L_{\text{Total\_Phen}} \quad (2)$$

Nitrophenol is produced from phenol by first producing a phenoxy radical which then reacts with  $\text{NO}_2$  with a 100% yield. The fraction of the phenol loss that produces nitrophenol ( $F_{\text{NPHEN}}$ ) was determined by dividing the production of the phenoxy +  $\text{NO}_2$  dummy species ( $P_{\text{PHENNPHEN}}$ ; see Table S1 in Supporting Information S1) by  $L_{\text{Total\_Phen}}$ , as shown in Equation 3:

$$F_{\text{NPHEN}} = P_{\text{PHENNPHEN}} / L_{\text{Total\_Phen}} \quad (3)$$

The same process was repeated for cresol to calculate the fractional production of methylcatechol versus nitrocresol from cresol loss. Total loss of cresol ( $L_{\text{Total\_Csl}}$ ) was calculated over the 2-month period as the total of the two loss tracers ( $L_{\text{OH\_Csl}} = \text{CSLOH}$  and  $L_{\text{NO}_3\text{\_Csl}} = \text{CSLNO}_3$ ) and total dry and wet deposition ( $L_{\text{DryDep\_Csl}}$  and  $L_{\text{WetDep\_Csl}}$ ), as shown in Equation 4:

$$L_{\text{Total\_Csl}} = L_{\text{OH\_Csl}} + L_{\text{NO}_3\text{\_Csl}} + L_{\text{DryDep\_Csl}} + L_{\text{WetDep\_Csl}} \quad (4)$$

The fraction of the cresol loss that produces methylcatechol ( $F_{\text{MCT}}$ ) was determined by multiplying  $L_{\text{OH\_Csl}}$  by the yield of methylcatechol from the cresol + OH reaction (0.727) and dividing the result by  $L_{\text{Total\_Csl}}$ , as shown in Equation 5:

$$F_{\text{MCT}} = (L_{\text{OH\_Csl}} \times 0.727) / L_{\text{Total\_Csl}} \quad (5)$$

Nitrocresol is produced from the phenoxy radical +  $\text{NO}_2$  reaction with a 100% yield. The fraction that produces nitrocresol ( $F_{\text{NCSL}}$ ) was determined by dividing the production of the phenoxy +  $\text{NO}_2$  dummy species ( $P_{\text{CSLNPHEN}}$ ; see Table S1 in Supporting Information S1) by  $L_{\text{Total\_Csl}}$ , as shown in Equation 6:

$$F_{\text{NCSL}} = P_{\text{CSLNPHEN}} / L_{\text{Total\_Csl}} \quad (6)$$

### 3. Evaluation of the GEOS-Chem Aromatic Simulation

#### 3.1. Baseline Simulation and Impacts of Model Resolution

Figure 3 shows the boundary layer vertical profiles of the observations for 7 aromatic compounds along with  $\text{NO}$  and  $\text{NO}_2$  and the baseline model simulations at three resolutions (two global, one nested; see Section 2.2) for 7 aromatic compounds along with  $\text{NO}_x$  ( $\text{NO}_x = \text{NO} + \text{NO}_2$ ) and  $\text{HO}_x$  ( $\text{HO}_x = \text{OH} + \text{HO}_2$ ). Vertical profiles for individual  $\text{NO}_x$ ,  $\text{HO}_x$ , and  $\text{OH}$  are shown in Figure S5 in Supporting Information S1. Consistent with prior KORUS-AQ analysis (Brewer et al., 2022; Simpson et al., 2020), toluene was the most abundant BTEX precursor species in the observations indicating high toluene emissions in the region. Benzene was the next most abundant, followed by ethylbenzene, then xylene. At the coarsest global resolution ( $4^\circ \times 5^\circ$ ), the baseline model overestimated benzene at all altitudes, but the simulation improved at the  $2^\circ \times 2.5^\circ$  and nested resolutions. Benzene was the only BTEX species with a non-zero mixing ratio above 2 km (not shown) as a result of its 8–10 days atmospheric lifetime, which is much longer than for the other species (2–24 hr) (Cabrera-Perez et al., 2016) and sufficiently long for emissions from elsewhere in Asia to be transported to South Korea. The baseline model replicates this feature well at all resolutions. We note that benzene's longer atmospheric lifetime makes it more sensitive than other species to our choice of spin-up period, especially in the global coarse resolution simulation. However, we found using a sensitivity simulation at  $4^\circ \times 5^\circ$  that a longer spin-up resulted in decreases that were

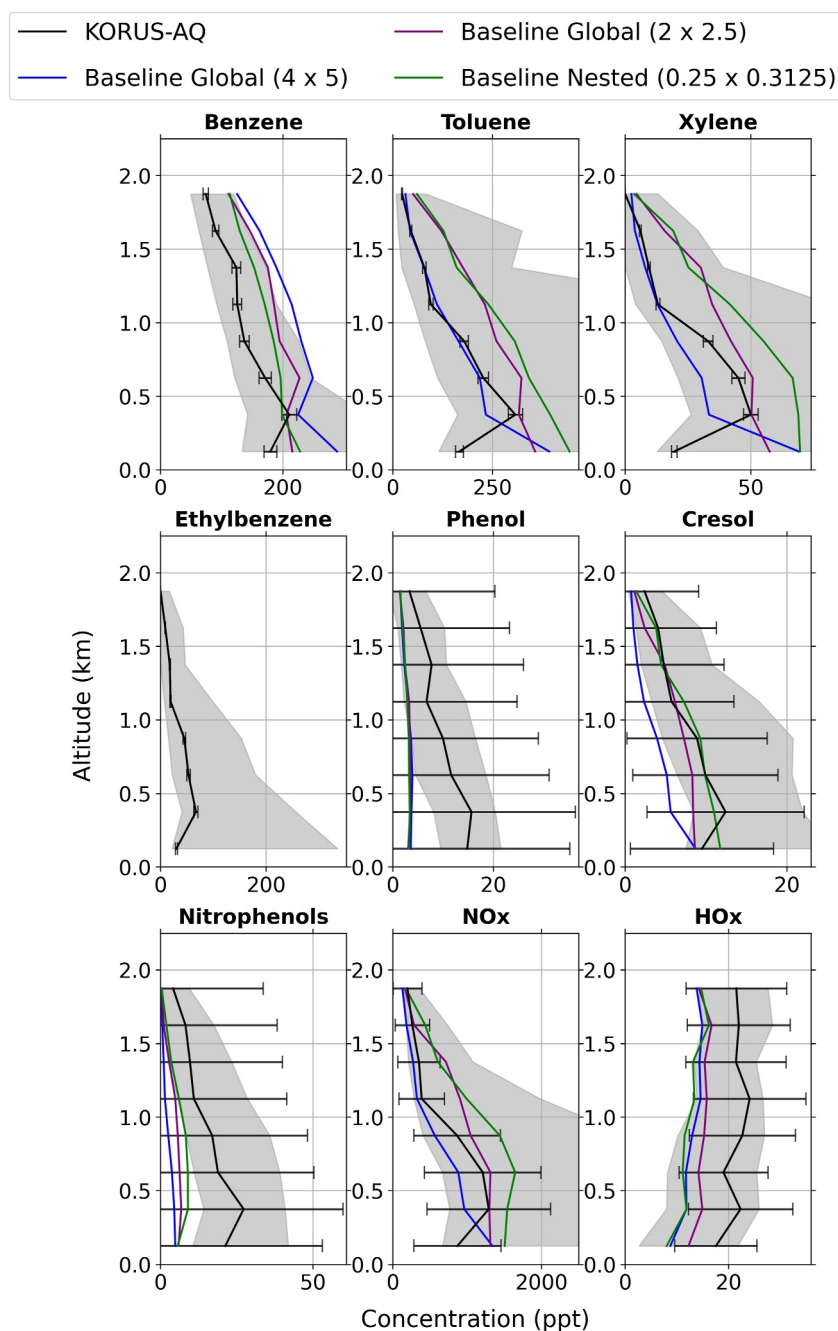


**Figure 3.** Median 0–2 km vertical profiles of benzene, toluene, xylene, ethylbenzene, phenol, cresol, nitrophenols,  $\text{NO}_x$ , and  $\text{HO}_x$  from the KORUS-AQ observations (black) compared with the GEOS-Chem baseline simulation at  $4^\circ \times 5^\circ$  (blue),  $2^\circ \times 2.5^\circ$  (purple), and  $0.25^\circ \times 0.3125^\circ$  (green) resolutions. For ethylbenzene, only observed values are shown as it was not included in the baseline simulations. Both observations and model output are binned into 250 m altitude bins. Error bars represent the observational uncertainties applied to the median values. Shaded areas represent the observational interquartile range.

smaller than the difference between resolutions (no change at the surface and a small decrease of  $\sim 25$  pptv at 1–2 km).

Table 2 shows the Pearson correlation coefficients ( $r$ ) and normalized mean biases (NMB) between the model and observations for the precursor species at all resolutions. Benzene, toluene, and xylene show increasing correlation as model resolution increases, highlighting the importance of resolution, as has been seen for methane (Stanevich



**Table 2**  
Pearson Correlation Coefficients ( $r$ ) and Normalized Mean Biases (NMB) at Three Resolutions for the Baseline GEOS-Chem Simulation<sup>a</sup>

Species	$r^b$			NMB (%)		
	4 × 5	2 × 2.5	Nested	4 × 5	2 × 2.5	Nested
Benzene	<b>0.83</b>	<b>0.88</b>	<b>0.90</b>	52	32	24
Toluene	0.69	<b>0.85</b>	<b>0.86</b>	13	63	85
Xylene	0.47	0.78	<b>0.85</b>	3	62	99
Phenol	<b>0.87</b>	0.76	<b>0.88</b>	−69	−70	−71
Cresol	<b>0.83</b>	<b>0.93</b>	<b>0.94</b>	−50	−18	2
Nitrophenols	<b>0.95</b>	<b>0.91</b>	<b>0.85</b>	−84	−71	−63
NO <sub>x</sub>	<b>0.82</b>	<b>0.89</b>	<b>0.93</b>	−14	30	54
HO <sub>x</sub>	<b>0.79</b>	<b>0.81</b>	0.65	−40	−30	−41

<sup>a</sup>Values calculated using data <2 km. <sup>b</sup>Bold numbers indicate results that are significant at a  $p$ -value < 0.05.

et al., 2020), isoprene and formaldehyde (Yu et al., 2016), SOA (Wainwright et al., 2012), and ozone in both GEOS-Chem and other models (Schwantes et al., 2022). For benzene, the model high bias decreases with increasing resolution, although benzene remains overestimated even at the highest resolution, most likely reflecting overestimated emissions. Modeled toluene and xylene both have almost no bias at the coarsest resolution, but the biases increase with increasing resolution, resulting in the model overestimating both species by nearly a factor of two in the nested simulation.

The fact that benzene concentrations decrease with increasing (finer) resolution while toluene and xylene concentrations increase may be explained by the differences in their atmospheric lifetimes. The longer atmospheric lifetime of benzene results in a larger contribution from emissions transported from China, meaning transport and numerical diffusion effects come into play. Coarser resolutions are more strongly affected by numerical diffusion, resulting in lower concentration maxima but larger plume sizes (Eastham & Jacob, 2017). It is likely that at coarser resolution, the flight tracks more frequently sample transported plumes (even if the concentrations within these plumes are lower), resulting in higher average concentrations of benzene over the South Korean region. Indeed, when we separate data over the Yellow Sea (primarily transported) from data over South Korea (primarily local), we see much stronger resolution effects for the transported data (Figure S6 in Supporting Information S1).

In contrast, toluene and xylene have much shorter atmospheric lifetimes than benzene and are therefore more strongly influenced by local emissions with high spatial variability. In coarse resolution simulations, the influence of large but spatially localized emissions is reduced due to the spatial averaging. These influences are better captured at the higher resolutions that average over a smaller area, explaining the increased concentrations at finer resolutions. Comparing the vertical profiles of these species over South Korea versus the Yellow Sea (Figure S6 in Supporting Information S1) confirms that the increases with resolution are only seen over South Korea, where the impacts from local emissions are strongest. Over the Yellow Sea, toluene and xylene concentrations decrease with increasing resolution, consistent with the pattern seen for benzene.

Amongst the measured aromatic oxidation products, Figure 3 shows that nitrophenols were most abundant in the KORUS-AQ observations. The observations show more phenol than cresol despite higher concentrations of toluene (cresol precursor) than benzene (phenol precursor), in part due to the lower yield and faster loss rates for cresol than phenol. The high phenol concentrations may also indicate a role for either primary phenol emissions or additional chemical sources of phenol besides benzene, both of which are explored in Section 4. The baseline simulation does not reproduce these observed patterns at any resolution. In all cases, modeled cresol is most abundant, followed by nitrophenols, then phenol. This disconnect, along with the large underestimate of phenol despite the overestimated benzene concentrations, indicates missing (or underestimated) sources of phenol and nitrophenols in the baseline simulation.

Table 2 shows that cresol is affected by increasing resolution, resulting in improvements to the observation-model correlation and reduced model biases with increasing resolution. Nitrophenols also show small improvements in

model biases with increasing resolution, but worse correlation. Conversely, phenol shows no change with resolution, with a low bias apparent at all resolutions, possibly due to the simultaneous decrease of benzene (the primary precursor) with increasing resolution, offsetting any potential resolution-driven increase in phenol. This result provides further evidence for missing sources of phenol, as the lack of improvement with higher resolution implies spatial variability in existing phenol sources is not the primary determinant of model skill in simulating phenol, unlike for the other aromatic species and oxidation products. Nevertheless, given the improvements at higher resolution simulated for most species, hereafter we exclusively discuss the high-resolution nested simulations.

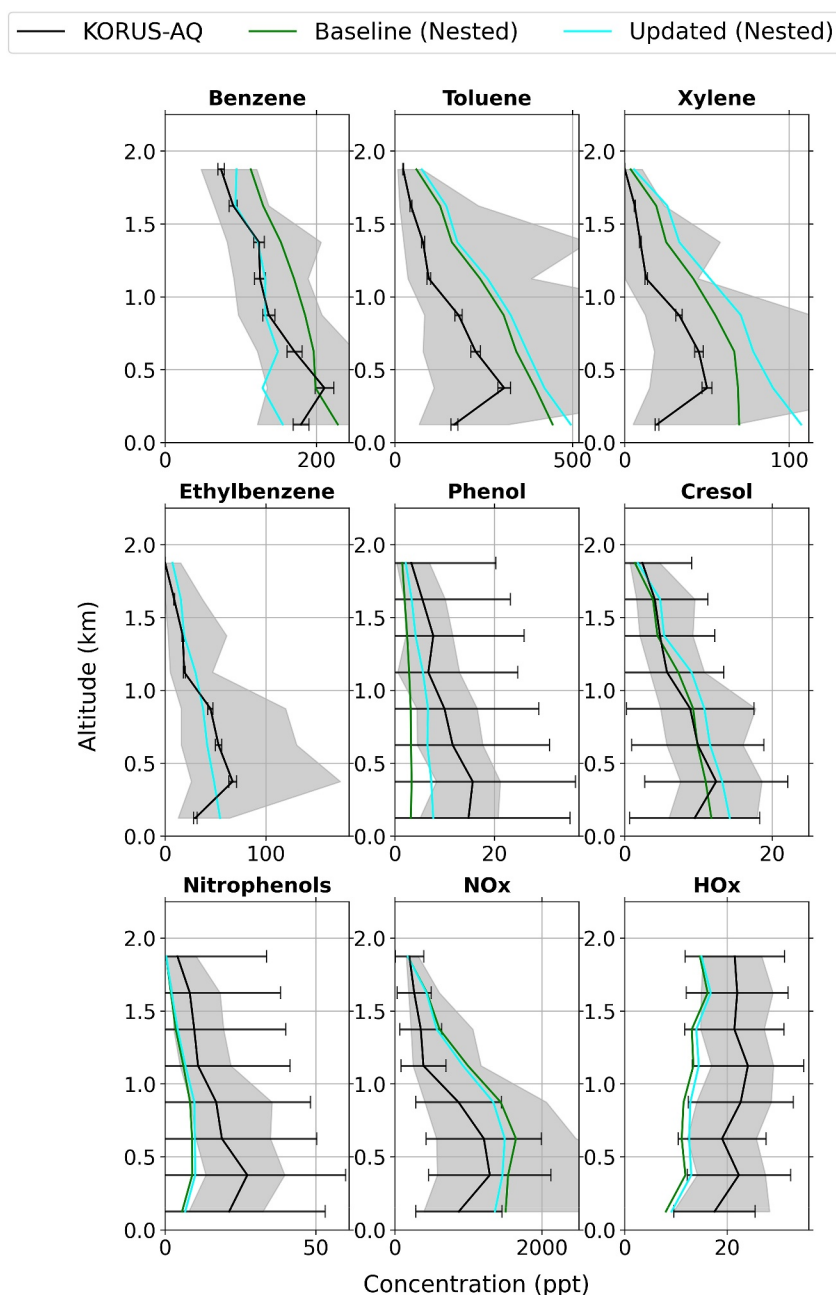
### 3.2. Impacts of Updated Emissions and Phenol Chemistry

Figure 4 and Table 3 show the impacts of the improvements made to the GEOS-Chem aromatic emissions and chemical mechanism, as detailed in Section 2.2.2, and Figure S7 in Supporting Information S1 shows the impacts to individual  $\text{HO}_x$ ,  $\text{NO}_x$ , and  $\text{O}_3$ . The updates resulted in notable changes to BTEX species, phenol, and cresol, with only negligible impacts on modeled nitrophenols. Benzene decreased by 73 ppt at the surface (and roughly 20–70 ppt throughout the boundary layer) in the updated simulation. The high bias in the original simulation was reduced from  $\text{NMB} = 24\%$  to  $\text{NMB} = -9\%$ , with the improvements driven by the updated aromatics (ARO1) emission speciation. Below 1 km, however, the improved model underestimates benzene, indicating underestimated local emissions and/or poorly represented vertical transport in the boundary layer. As discussed further in Section 3.3, the surface-level benzene is primarily associated with local emissions from Seoul and Daesan, with some influence from transport from China.

For toluene, the impacts were smaller due to the contrasting effects of the decrease in emissions from the updated ARO1 speciation and the addition of new toluene emissions from VCPs. Combined, these changes resulted in a moderate increase in atmospheric toluene, particularly in surface air. Across the lowest 2 km, the model bias increased from  $\text{NMB} = 85\%$  to  $\text{NMB} = 102\%$ . Modeled xylene mixing ratios, which were already overestimated in the baseline simulation ( $\text{NMB} = 99\%$ ), also increased due to the addition of VCP emissions, resulting in an increased bias ( $\text{NMB} = 163\%$ ). Observation-model correlation of xylene decreased from 0.85 to 0.75, indicating that our simple population-based representation of xylene VCP emissions is not well-suited to South Korea. Modeled ethylbenzene, a new addition in the updated simulation, was reasonably well correlated with observations ( $r = 0.81$ ) and had only a small positive bias ( $\text{NMB} = 6\%$ ), indicating good agreement with the observations. Remaining uncertainties in BTEX emissions are further explored in Section 3.3.

Despite the decrease in benzene concentrations, the improved simulation resulted in a substantial increase in phenol concentrations, reducing the model bias from  $\text{NMB} = -71\%$  to  $\text{NMB} = -42\%$ . The correlation between modeled and observed phenol also improved ( $r = 0.92$ ). When separating the data over South Korea from that over the Yellow Sea (see Figure S8 in Supporting Information S1), we found that modeled phenol increased substantially over land, but showed minimal improvement over the Yellow Sea. This may be due to the larger toluene overestimates over land producing more phenol, or due to phenol oxidizing before reaching the Yellow Sea. We also found larger phenol biases over the Yellow Sea ( $\text{NMB} = -73\%$ ) than over South Korea ( $\text{NMB} = -33\%$ ). As simulated benzene is also significantly underestimated over the Yellow Sea but agrees well with observations over South Korea, we infer that transported benzene emissions (likely from China) are underestimated and can account for the underestimated phenol over the Yellow Sea. These results indicate that phenol concentrations over the Yellow Sea are more heavily impacted by transported benzene emissions while phenol in South Korea is impacted more by local toluene and ethylbenzene emissions. We found using sensitivity simulations (see Figure S9 in Supporting Information S1) that the additional primary emissions of phenol had negligible impact, and the increased phenol can be almost entirely attributed to the addition of phenol production from toluene and ethylbenzene oxidation. Our results lend further evidence to the possible importance of these phenol production pathways that have previously been identified in lab studies (Birdsall & Elrod, 2011; Forstner et al., 1997; Noda et al., 2009).

The modeled cresol bias increased from  $\text{NMB} = 2\%$  to  $\text{NMB} = 23\%$  due to the increase in toluene and xylene; however, modeled cresol was still well within the observational uncertainties and strongly correlated with observed cresol ( $r = 0.94$ ). Cresol is overestimated over South Korea but underestimated over the Yellow Sea (Figure S8 in Supporting Information S1), despite toluene and xylene overestimates in both regions. This might indicate missing photochemical sources of cresol in transported plumes or that the atmospheric lifetime of cresol



**Figure 4.** Same as Figure 3, but for the high-resolution (nested) baseline (green) and improved (cyan) simulations.

is too short in the model. Correction of the toluene and xylene overestimates would likely improve the cresol simulation over South Korea but degrade it over the Yellow Sea, where cresol is already too low. Future work is needed to fully assess the model performance for cresol.

We found almost no changes between the baseline and improved simulations of nitrophenols, which remain underestimated (although within the experimental uncertainties) in the improved simulation despite the increases to the nitrophenol precursors (phenol and cresol) and lingering model overestimates of  $\text{NO}_x$ . As seen for phenol, simulated nitrophenols are more representative of the observations over South Korea than over the Yellow Sea. While observations show roughly equivalent concentrations over the two regions, virtually no nitrophenol is simulated over the Yellow Sea. This may be due to the underestimated precursors (phenol and cresol) over the Yellow Sea, as well as the underestimate of transported benzene. The atmospheric lifetime of nitrophenols may

**Table 3**

The Same as Table 2, but for the Nested Baseline and Updated Simulations<sup>a</sup>

Species	<i>r</i> <sup>b</sup>		NMB (%)	
	Baseline	Updated	Baseline	Updated
Benzene	<b>0.90</b>	<b>0.79</b>	24	−9
Toluene	<b>0.86</b>	<b>0.84</b>	85	102
Xylene	<b>0.85</b>	<b>0.75</b>	99	163
Ethylbenzene	−	<b>0.81</b>	−	06
Phenol	<b>0.88</b>	<b>0.92</b>	−71	−42
Cresol	<b>0.94</b>	<b>0.94</b>	2	23
Nitrophenols	<b>0.85</b>	<b>0.85</b>	−63	−58
NO <sub>x</sub>	<b>0.85<sup>b</sup></b>	<b>0.93</b>	54	43
HO <sub>x</sub>	0.65	0.68	−41	−37 <sup>a</sup>

<sup>a</sup>Values calculated using data <2 km. <sup>b</sup>Bold numbers indicate results that are significant at a *p*-value <0.05.

also be too low. Further, the lack of sensitivity to changes in precursors indicates that there may be missing nitrophenol sources in our mechanism. In contrast to the nitrophenol underestimates found here, a box model study using the Master Chemical Mechanism (MCM v3.2) overpredicted nitrophenols in the Uintah Basin, US (Yuan et al., 2016). This difference is likely due to the slower reaction rate of nitrophenol in the MCM ( $9 \times 10^{-13} \text{ cm}^3 \text{ molec}^{-1} \text{ s}^{-1}$  to OH;  $9 \times 10^{-14} \text{ cm}^3 \text{ molec}^{-1} \text{ s}^{-1}$  to NO<sub>3</sub>) as compared with our simulations ( $3.47 \times 10^{-12} \text{ cm}^3 \text{ molec}^{-1} \text{ s}^{-1}$  to OH;  $2.6 \times 10^{-12} \text{ cm}^3 \text{ molec}^{-1} \text{ s}^{-1}$  to NO<sub>3</sub>), which use the nitrocatechol reaction rates.

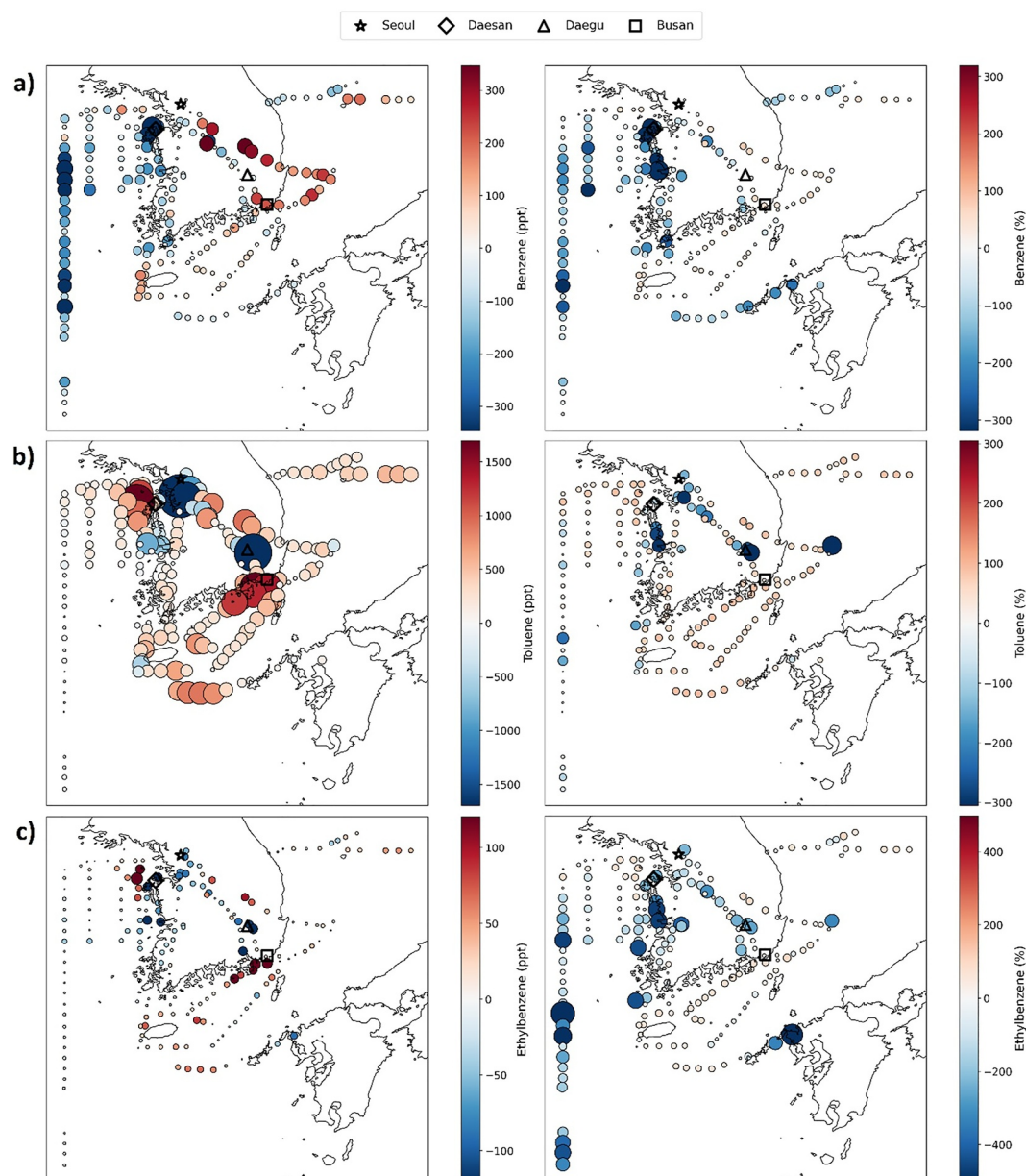
### 3.3. Remaining Uncertainties in Aromatic Emissions

Figure 5 shows the absolute differences between the updated model and the observations along the flight track below 1 km for benzene, toluene, and ethylbenzene. Xylene shows similar patterns to toluene (see Figure S10 in Supporting Information S1) and as such is not discussed here. The spatial patterns of the biases show differences in the relationships between different BTEX species associated with different source regions. These differences imply applying a single ARO1 emission speciation to all KORUSv5 emissions does not adequately reflect the different emission sources across South Korea and hint at areas for future inventory improvement.

As shown in Figure 5, we find that the model underestimates benzene and to a lesser extent ethylbenzene near the Daesan petrochemical complex in the northwest while overestimating toluene and xylene in this region. This result indicates that the benzene-to-toluene ratio implemented in the updated run (i.e., ARO1 speciation of 1.3% benzene, 86.6% toluene) is likely too low for petrochemical source emissions. A higher ratio would be more appropriate for the Daesan petrochemical complex. This pattern of difference is unique to the Daesan area.

In the areas south of Seoul and around Daegu, all species are biased low in the model, indicating underestimates of total aromatic emissions. In these regions, the underestimate is largest for toluene, implying a larger correction would be necessary for toluene than for benzene (and therefore, a lower benzene-to-toluene emission ratio). Conversely, the model overestimates all species at Busan, an area with high emissions as shown in Figure 2, with the largest high biases for toluene. The model overestimates in the Busan region may be caused by emissions from Ulsan, another petrochemical complex located to the northeast of Busan. The similarity to the large overestimate in toluene from Daesan indicates a potential general overestimate of aromatic emissions from petrochemical sources in the KORUSv5 inventory. At Daegu, the large toluene underestimate may be due to emissions from the Daegu dyeing industrial complex. While significant toluene emissions from Daegu have been reported previously (Shuai et al., 2018), simulated toluene emissions in the region are relatively low as shown in Figure 2b. Ethylbenzene is also underestimated in the Daegu region, although to a lesser extent than toluene.

Figure 5a shows that the model underestimates benzene over the Yellow Sea, west of Daesan. Data in this region were collected during several flights that sampled pollution transported from China (mostly Shanghai) (NASA, 2016). The large model biases in this region indicate underestimates of benzene transported from China, which could reflect a combination of underestimated Chinese emissions and model uncertainties in transport. Transport from the Seoul plume also impacted the data collected in the Yellow Sea region (NASA, 2016), and so the large benzene biases may be exacerbated by emissions underestimates from Seoul and/or Daesan. Figure 5b shows that toluene has large overestimates in the Yellow Sea region, particularly close to Daesan during flights that sampled the Seoul plume rather than flights that sampled transport from China. As we have found a large toluene underestimate in the Seoul Metropolitan Area, the biases in the Yellow Sea area are more likely associated with overestimated emissions from Daesan. Figure 5c shows that the spatial patterns of ethylbenzene performance in the Yellow Sea are similar to those for benzene (but smaller in magnitude), with underestimates in regions most likely influenced by transport from China and overestimates near Daesan.



**Figure 5.** Absolute (left) and relative (right) difference between the updated model and the observations along the KORUS-AQ flight track below 1 km for (a) benzene, (b) toluene, and (c) ethylbenzene. Both circle size and color indicate the magnitude of the difference. Red colors indicate model overestimates, and blue colors indicate model underestimates.

## 4. Atmospheric Budgets of Aromatic Oxidation Products

### 4.1. Phenol

Table 4 shows the overall 0–2 km budget for phenol during May–June 2016 as calculated by GEOS-Chem. We find benzene oxidation is the dominant phenol source at just over 40% ( $818 \text{ Mg month}^{-1}$ ) of total monthly production. This is closely followed by toluene at 40% ( $809 \text{ Mg month}^{-1}$ ), ethylbenzene at 11% ( $226 \text{ Mg month}^{-1}$ ), and lastly direct emissions at 9% ( $174 \text{ Mg month}^{-1}$ ). These results indicate that both toluene and ethylbenzene can be important sources of phenol, despite their lower phenol yields compared to benzene. We note that correction of the remaining model biases in benzene and toluene (see Section 3.3) would increase the phenol contribution from benzene oxidation and decrease the contribution from toluene oxidation, but toluene oxidation would remain an atmospherically relevant pathway. Phenol loss pathways in the boundary layer are



**Table 4**  
*Atmospheric Budget of Phenol Over South Korea During KORUS-AQ, as Calculated by GEOS-Chem<sup>a</sup>*

Sources					
	Emissions	Benzene	Toluene	Ethylbenzene	Total
Mg month <sup>-1</sup>	174	818	809	226	2,027
%	8.6	40.4	40.0	11.1	
Sinks					
	OH	NO <sub>3</sub>	Dry deposition	Wet deposition	Total
Mg month <sup>-1</sup>	1,463	446	54	32	1,995
%	73.3	22.4	2.7	1.6	

<sup>a</sup>Summed over May–June 2016, latitude 32.9°–39°N, longitude 125.5°–129.8°E, altitude 0–2 km.

dominated by reaction with OH, accounting for 73% (1,463 Mg month<sup>-1</sup>) of total loss, followed by reaction with NO<sub>3</sub> (22%; 446 Mg month<sup>-1</sup>) and dry deposition (2.7%; 54 Mg month<sup>-1</sup>). We note that the NO<sub>x</sub> overestimate shown in Section 3.2 may result in overestimates in both NO<sub>3</sub> concentrations and phenol loss to NO<sub>3</sub> (as well as other aromatic oxidation products), which may also partly account for the continued underestimates of phenol in the model. This remains an uncertainty in our simulation.

The diel variation of each production and loss pathway at the surface shown in Figure 6. Figure 6a shows that the surface production of phenol is largest at midday, when photochemical processes are active. We find that emissions are the largest surface-layer phenol source throughout the day. This is followed by toluene oxidation, benzene oxidation, and finally ethylbenzene oxidation. Figure 6b shows that the primary loss pathway for phenol in surface air is through reaction with OH. This is followed by reaction with NO<sub>3</sub>, dry deposition, and finally wet deposition. Surface-level phenol loss is highest in the middle of the day due to increased OH production from O<sub>3</sub> photolysis. Reaction with NO<sub>3</sub> is the major loss pathway at night. The model simulates a secondary peak in phenol

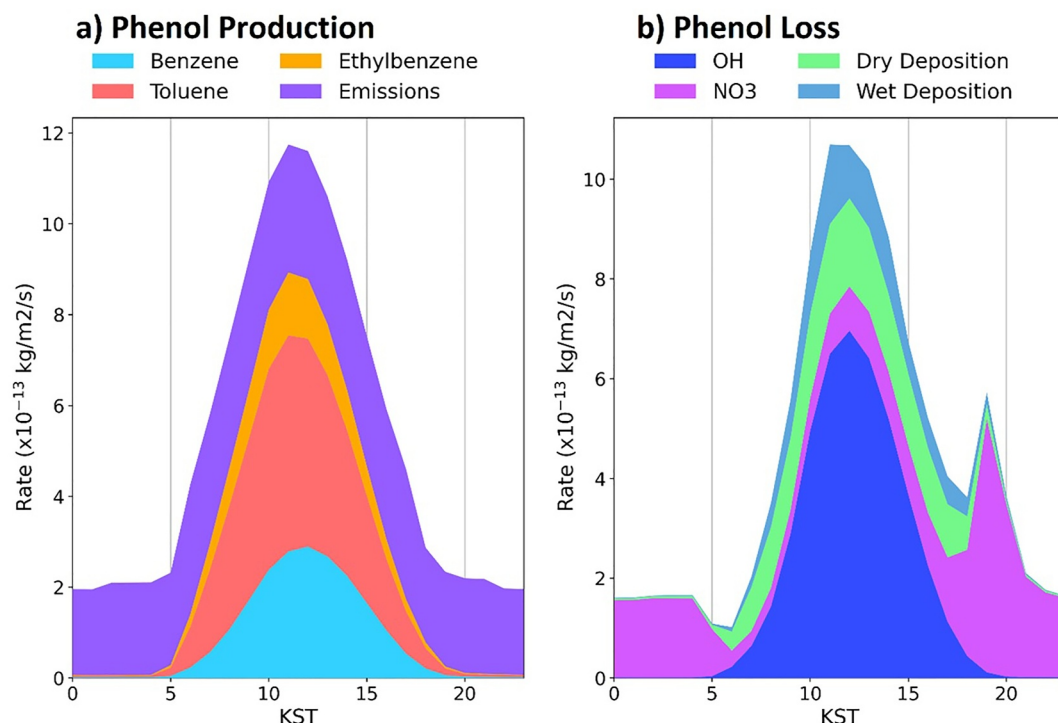


**Figure 6.** Surface level diel variations of phenol (a) production and (b) loss pathways simulated by GEOS-Chem, averaged over May and June 2016 between latitude 32.9°–39°N and longitude 125.5°–129.8°E.

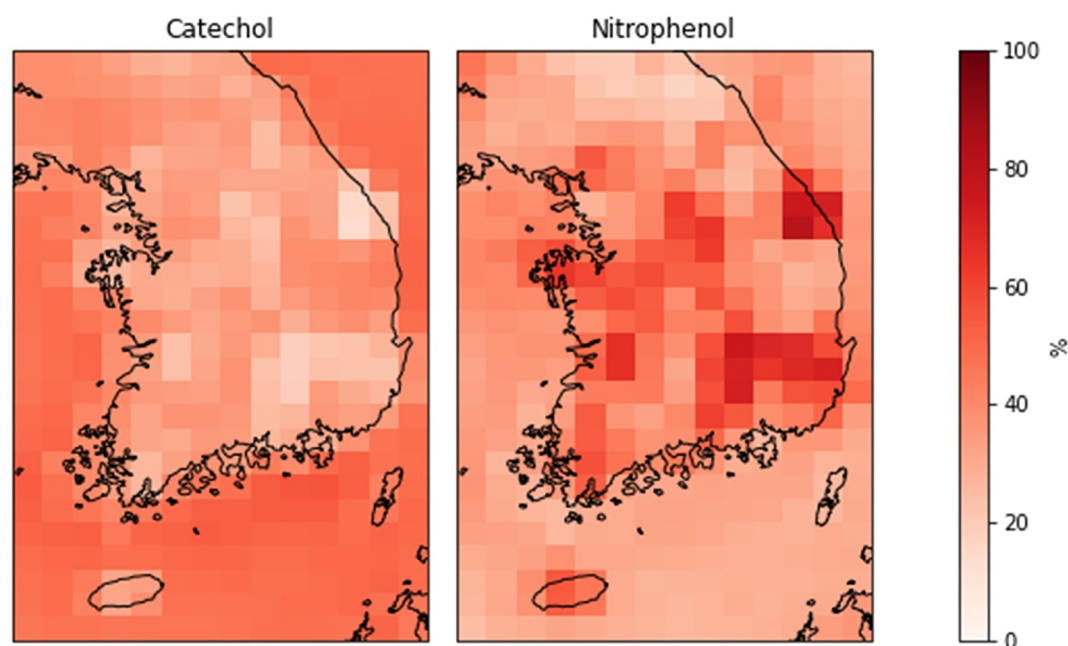


**Figure 7.** The percentage of phenol loss that produces (a) catechol and (b) nitrophenol in surface air, averaged over May–June 2016, as simulated by GEOS-Chem.

loss to  $\text{NO}_3$  in the late evening ( $\sim 19:00$  KST), which we find is caused by increasing  $\text{NO}_3$  that drives an initial increase in phenol loss, followed by a rapid decline as phenol is removed by  $\text{NO}_3$  more rapidly than it is produced at this time of day.

Yuan et al. (2016) also explored diel cycles of phenol loss pathways. They used a box model driven by the Master Chemical Mechanism (MCMv3.2) to analyze surface-level phenol loss from the Uintah Basin in the US during winter. Although their analysis was for a very different location and at a different time of year, they similarly found that chemical loss dominates over deposition as a phenol sink and that chemical loss is mostly to OH during the day and to  $\text{NO}_3$  at night. In contrast to our finding that OH dominates phenol loss over South Korea (both at the surface and within the boundary layer), their results showed phenol loss to OH and  $\text{NO}_3$  were roughly balanced ( $21 \text{ ppt d}^{-1}$  for OH,  $19 \text{ ppt d}^{-1}$  for  $\text{NO}_3$ ). This difference is likely due to our results being averaged over a larger area, which includes remote low- $\text{NO}_x$  regions (i.e., over water), as well as higher OH and longer days during summer. We tested this by also calculating our modeled loss rates using data over land only and found closer equivalence between OH and  $\text{NO}_3$  as drivers of phenol loss, consistent with Yuan et al. This result indicates similar phenol chemistry between different regions (US, Korea) and seasons (winter, summer).

Figure 7 compares the fates of phenol oxidation in surface air in terms of the relative production of the catechol and nitrophenol secondary oxidation products (see Section 2.3). The figure shows that the dominant species produced from phenol oxidation varies spatially. We find that catechol is the major product in low- $\text{NO}_x$  remote regions and over the ocean, with nitrophenol dominant over high- $\text{NO}_x$  urban and industrial areas. Nitrophenol production increases with  $\text{NO}_x$  concentration (see Figure S11 in Supporting Information S1) as nitrophenol production requires the phenoxy radical intermediate (produced from phenol reacting with  $\text{NO}_3$  or OH) to react with  $\text{NO}_2$ . The nitrophenol production pathway is important even though phenol loss to OH dominates over loss to  $\text{NO}_3$ . Nitrophenol production is further discussed in Section 4.3.

#### 4.2. Lumped Cresols

Table 5 shows the overall 0–2 km budget for lumped cresols (cresol and xylenol) as simulated by GEOS-Chem. There are few direct sources of cresols, and we find emissions provide the smallest contribution to lumped cresol sources, accounting for 1.5% ( $75 \text{ Mg month}^{-1}$ ) of monthly boundary layer sources. Simulated cresols production in the boundary layer is dominated by toluene at 63% ( $3,269 \text{ Mg month}^{-1}$ ) followed by xylene at 35% ( $1,824 \text{ Mg month}^{-1}$ ). The contribution from xylene in our simulations represents xylenol (15% xylenol yield from

**Table 5**

Atmospheric Budget of Lumped Cresols Over South Korea During KORUS-AQ as Calculated by GEOS-Chem<sup>a</sup>

Sources					
	Emissions	Toluene	Xylene	Total	
Mg month <sup>-1</sup>	75.3	3,269	1,824	5,168	
%	1.5	63.3	35.3		
Sinks					
	OH	NO <sub>3</sub>	Dry deposition	Wet deposition	Total
Mg month <sup>-1</sup>	3,986	1,328	85.3	56.7	5,456
%	73.1	24.3	1.6	1.0	

<sup>a</sup>Summed over May–June 2016, latitude 32.9°–39°N, longitude 125.5°–129.8°E, between 0 and 2 km.

xylene oxidation by OH), which the mechanism lumps with cresol. Direct production of cresol from xylene has been reported with a 4.3%–11.2% yield, depending on the isomer (Noda et al., 2009). However, we did not include this pathway in our simulations given conflicting evidence that suggests an upper limit of 1% cresol yield from m-xylene (Aschmann et al., 2010). Simulated cresols loss in the boundary layer is dominated by oxidation reaction with OH at 73% (3,986 Mg month<sup>-1</sup>), followed by reaction with NO<sub>3</sub> at 24% (1,328 Mg month<sup>-1</sup>), dry deposition at 2% (85 Mg month<sup>-1</sup>), and wet deposition at 1% (57 Mg month<sup>-1</sup>).

The average diel contributions to production and loss at the surface shown in Figure 8. As for phenol, production peaks at midday and is negligible at night. Surface layer contributions are similar to production in the boundary layer, with a slightly larger role for emissions. Lumped cresol loss is largest at midday, as seen in Figure 8b, and dominated by reaction with OH. This is followed by reaction with NO<sub>3</sub>. We find that dry and wet deposition are less important for lumped cresols at the surface than for phenol. Night-time loss to

reaction with NO<sub>3</sub> is also found to be less important for lumped cresols than for phenol, and there is no secondary peak in cresol loss in the evening. We find this difference between species arises because the modeled lumped cresol concentrations decrease more rapidly than phenol throughout the afternoon (declining ~1 hr earlier in the day; see Figure S12 in Supporting Information S1) due to the faster reaction rates with OH and NO<sub>3</sub> for cresols than for phenol. As a result, by the time NO<sub>3</sub> concentrations increase in the evening, there is little remaining cresol in surface air, and so we do not see the short-term increase in loss to NO<sub>3</sub> that was simulated for phenol.

Figure 9 compares the fates of lumped cresols in surface air in terms of their relative likelihood of forming methylcatechol vs. nitrocresol. We find that there is little spatial variation in these two fates. Averaged over the region shown in Figure 9 during May–June 2016, 56% of cresol loss forms methylcatechol and 46% forms nitrocresol. The difference between the variation in cresol products and phenol products is likely due to the cresol + OH/NO<sub>3</sub> reaction rates being more similar to one another than the phenol + OH/NO<sub>3</sub> rates, as well as the lack of a secondary peak in loss to NO<sub>3</sub> as previously discussed.

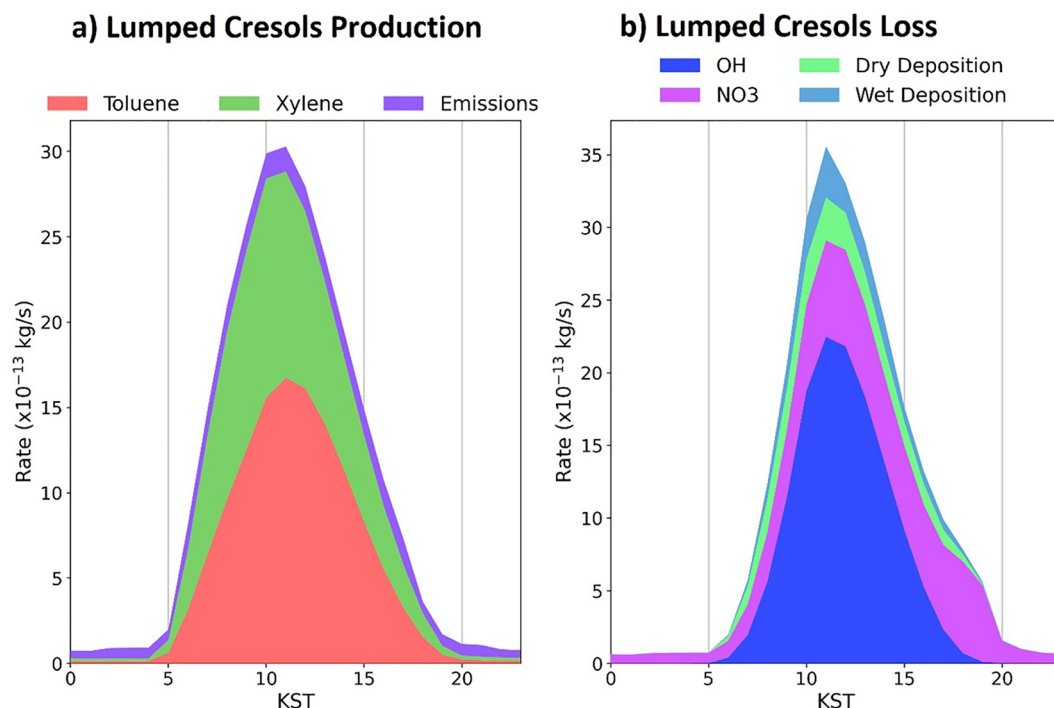


**Figure 8.** The same as Figure 6, but for lumped cresols (a) production and (b) loss pathways, as simulated by GEOS-Chem.

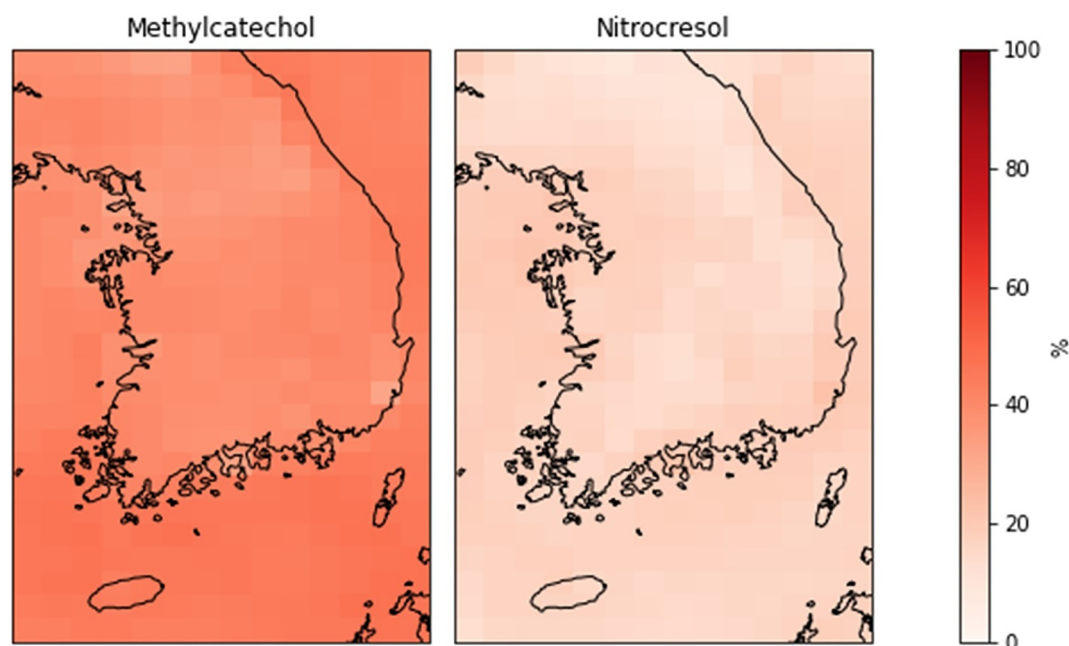


**Figure 9.** The percentage of cresol loss that produces (a) methylcatechol and (b) nitroresol in surface air, averaged over May–June 2016, as simulated by GEOS-Chem.

### 4.3. Nitrophenol

Table 6 provides the contributions to nitrophenol production from phenol and benzaldehyde oxidation in surface air as simulated by GEOS-Chem, with the diel cycles shown in Figure 10. We find benzaldehyde is the dominant source of nitrophenol production (67% from benzaldehyde, 33% from phenol), with benzaldehyde the dominant source during the day and phenol the dominant source at night. We note that the benzaldehyde contribution simulated here may be overestimated given the overestimate in toluene, which produces benzaldehyde with a 6% yield.

Yuan et al. (2016) performed a similar analysis but for production of phenoxy radicals, which go on to form nitrophenols via reaction with  $\text{NO}_2$ . Consistent with our results for nitrophenols, they found that phenol oxidation was the largest night-time source of phenoxy radicals. They also found an overall contribution from phenol at 29%, consistent with our results here. In their simulation, the largest source was phenylperoxy radicals, but they did not differentiate the sources of these radicals, which can come from both benzaldehyde and phenol oxidation. Our results go a step further, as we tracked the full pathway from phenol and benzaldehyde to nitrophenols, including differentiating the source of the phenylperoxy radicals (see Section 2.3 and Table S1 in Supporting Information S1). From this we find that benzaldehyde, a nitrophenol precursor not quantified previously, is an important chemical source of nitrophenol.

## 5. Conclusions

We have used airborne observations from the KORUS-AQ campaign over South Korea to better understand the emissions and chemistry of aromatics and their oxidation products (phenol, cresols, and nitrophenol). We first used the observations to evaluate the aromatic chemical mechanism in the GEOS-Chem v13.4.0 chemical transport model at three resolutions (two global, one nested). This analysis, along with recent findings from other studies, guided the implementation of several changes to the model, including updating existing emission speciation, adding emission sources, and including additional chemical reactions. From there, we used the updated model at  $0.25^\circ \times 0.325^\circ$  resolution to quantify the atmospheric budgets of phenol, lumped cresols, and nitrophenol in the South Korean boundary layer.

**Table 6**  
Sources of Nitrophenols Over South Korea During KORUS-AQ as Calculated by GEOS-Chem<sup>a</sup>

Sources	Phenol	Benzaldehyde	Total
Mg month <sup>−1</sup>	590	1,190	1,780
%	33.1	66.9	

<sup>a</sup>Summed over May–June 2016, latitude 32.9°–39°N, longitude 125.5°–129.8°E, between 0 and 2 km.

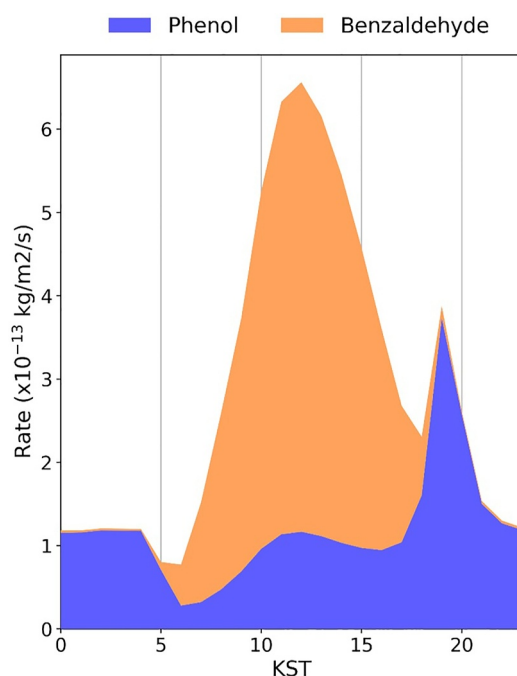


**Figure 10.** The same as Figure 6, but for nitrophenol production from phenol and benzaldehyde.

Our initial evaluation of the baseline model using KORUS-AQ measurements showed that the global GEOS-Chem simulation at  $4^\circ \times 5^\circ$  resolution overestimates benzene and largely underestimates the oxidation products but agrees well with observed toluene and xylene above the surface layer. We found that toluene, xylene, cresol, and lumped nitroaromatic concentrations increased with increasing (finer) model resolution, while benzene decreased. This resulted in better agreement with observations for cresol, nitroaromatics, and benzene, but worse agreement for toluene and xylene. We found that simulated phenol concentrations were not sensitive to changes in resolution, indicating potential missing sources.

Our updated simulation included additional sources of emissions for BTEX and phenol, ethylbenzene chemistry, and production of phenol from toluene and ethylbenzene oxidation. We found that adding ethylbenzene chemistry and including a direct phenol source from ethylbenzene and toluene oxidation substantially improved the agreement between observed and simulated phenol, reducing the model normalized mean bias from  $-71\%$  to  $-42\%$ . The changes to emissions improved simulation of benzene, but it remained somewhat too low below 1 km. Toluene showed minimal change between the baseline and updated simulations due to contrasting effects of the speciation updates and the new VCP emissions while xylene increased somewhat. Both toluene and xylene remain higher than observed in our updated simulation. These biases appear to be associated with industrial petrochemical emission overestimates in Ulsan and Daesan and underestimates from the Daegu dyeing industrial complex and the region south of Seoul. For benzene,

transported sources from China also appear to be too low, although this could reflect errors in emissions and/or transport. We found simulated nitroaromatics remained biased low relative to observations in the updated simulation, despite increases to phenol and cresol (nitroaromatic precursors). The lack of sensitivity of simulated nitroaromatics to the changes in aromatic precursors implies potential missing sources or chemistry that merit future investigation.

We find in the model that emissions and secondary production contribute approximately equal sources of phenol in surface air. Averaged over the boundary layer (0–2 km), emissions play a lesser role, accounting for only 9% of production. Benzene and toluene oxidation contribute equally at 40% each, followed by ethylbenzene oxidation at 11%. These results, along with the reduced model bias in the updated simulation, provide evidence that toluene and ethylbenzene are atmospherically relevant phenol precursors. The primary phenol sink in the boundary layer is loss by OH oxidation at 73%, followed by  $\text{NO}_3$  oxidation at 22%, then deposition at 5%. Reaction with OH is the major loss pathway during the day and reaction with  $\text{NO}_3$  is the major loss pathway at night. We find nitrophenol to be the major product of phenol oxidation in surface air in urban and industrial regions with high  $\text{NO}_x$  concentrations, whereas catechol is the major product in more remote regions and over the ocean where  $\text{NO}_x$  is lower.

We find lumped cresols primarily derive from secondary production, with toluene oxidation accounting for 63% of monthly production, followed by xylene oxidation at 35%, and emissions at 2%. The contribution from xylene represents xylenol, which is lumped with cresol in the model and may account for part of the cresol model bias in the updated simulation. Lumped cresol loss is also dominated by OH oxidation, accounting for 73% of monthly loss, followed by oxidation by  $\text{NO}_3$  (24%), dry deposition (2%), and wet deposition (1%). We find little spatial variability in cresol products, with methylcatechol and nitrocresol produced in approximately equal amounts in both urban high- $\text{NO}_x$  and remote low- $\text{NO}_x$  environments, likely due to the similarity in cresol reaction rates (in contrast to the more variable phenol reaction rates).

We find nitrophenol is produced dominated by benzaldehyde (phenol: 33%, benzaldehyde: 67%). We also find that benzaldehyde is the major daytime source of nitrophenol and phenol is the major nighttime source. Our simulation does not include direct nitrophenol emissions, which have recently been found to account for up to  $\sim 90\%$  of nitrophenol sources (Ahmed et al., 2023; Peng et al., 2023). Given that simulated nitrophenol showed little sensitivity to changes in precursors in our updated simulation, the addition of direct nitrophenol emissions in future could potentially resolve the low model biases seen here.



Previous laboratory studies have identified toluene and ethylbenzene as potential precursors of phenol (Birdsall & Elrod, 2011; Forstner et al., 1997; Noda et al., 2009). Our results showed improved agreement between model and observations with these sources included, suggesting they could be atmospherically relevant phenol sources and implying previous modeling studies may have underestimated atmospheric concentrations of phenol and its oxidation products in aromatic-rich environments. However, even with these sources, phenol remains underestimated in the model, and additional unidentified phenol sources may also be important. Further, we found that nitrophenol is the predominant product of phenol oxidation in urban environments. Combined, these results indicate that control of BTEX emissions is important for limiting the impact of highly toxic nitrophenols in highly populated regions with substantial aromatic emissions, like South Korea.

## Data Availability Statement

The KORUS-AQ measurements are available publicly (NASA, 2025). The model used in the study is based on GEOS-Chem v13.4.0, which is publicly available (The International GEOS-Chem User Community, 2022). Files used in the updated nested GEOS-Chem simulation are also publicly available (MacFarlane, 2025). Updates described here will be submitted for inclusion in future versions of the standard model following acceptance of this paper.

## Acknowledgments

We would like to thank Katherine Travis for input regarding ARO1 emission speciation, CO emissions, and HO<sub>2</sub> uptake. We would also like to thank Andrew Weinheimer, who provided the KORUS-AQ NO and NO<sub>2</sub> measurements that are used here, and Jared Brewer who provided code for creating the planeflight input files for GEOS-Chem. Support for this project includes funding from an Australian Government Research Training Program Scholarship, the National Aeronautics and Space Administration project 20-ACCDAM20-0039, the Research Grants Council of the Hong Kong Special Administrative Region, China, Early Career Scheme under Project Number CUHK 24300924, the Fine Particle Research Initiative in East Asia Considering National Differences (FRIEND) Project through the National Research Foundation of Korea (NRF) funded by the Ministry of Science and ICT under project code 2020M3G1A1114621. The work was undertaken with the assistance of resources provided at the NCI National Facility systems at the Australian National University through the National Computational Merit Allocation Scheme supported by the Australian Government (projects m19, q90). Open access publishing facilitated by University of Wollongong, as part of the Wiley - University of Wollongong agreement via the Council of Australian University Librarians.

## References

- Ahmed, M., Rappenglueck, B., Ganranoo, L., & Dasgupta, P. K. (2023). Source apportionment of gaseous Nitrophenols and their contribution to HONO formation in an urban area. *Chemosphere*, 338, 139499. <https://doi.org/10.1016/j.chemosphere.2023.139499>
- Allen, H. M., Crounse, J. D., Kim, M. J., Teng, A. P., Ray, E. A., McKain, K., et al. (2022). H<sub>2</sub>O<sub>2</sub> and CH<sub>3</sub>OOH (MHP) in the remote atmosphere: 1. Global distribution and regional influences. *Journal of Geophysical Research: Atmospheres*, 127(6), e2021JD035701. <https://doi.org/10.1029/2021JD035701>
- Andreae, M. O. (2019). Emission of trace gases and aerosols from biomass burning – An updated assessment. *Atmospheric Chemistry and Physics*, 19(13), 8523–8546. <https://doi.org/10.5194/acp-19-8523-2019>
- Aschmann, S. M., Arey, J., & Atkinson, R. (2010). Extent of H-atom abstraction from OH+p-cymene and upper limits to the formation of cresols from OH+m-xylene and OH+p-cymene. *Atmospheric Environment*, 44(32), 3970–3975. <https://doi.org/10.1016/j.atmosenv.2010.06.059>
- Baltaretu, C. O., Lichtman, E. I., Hadler, A. B., & Elrod, M. J. (2009). Primary atmospheric oxidation mechanism for toluene. *The Journal of Physical Chemistry A*, 113(1), 221–230. <https://doi.org/10.1021/jp806841t>
- Bates, K. H., Jacob, D. J., Li, K., Ivatt, P. D., Evans, M. J., Yan, Y., & Lin, J. (2021). Development and evaluation of a new compact mechanism for aromatic oxidation in atmospheric models. *Atmospheric Chemistry and Physics*, 21(24), 18351–18374. <https://doi.org/10.5194/acp-21-18351-2021>
- Bates, K. H., Specht, I., Jacob, D., Hornbrook, R., & Apel, E. C. (2022). Sources and chemistry of ethanol. Retrieved from <https://geos-chem.seas.harvard.edu/files/acmg-geos/files/igc10-d1-p07-bates.pdf>
- Bejan, I. G., Olariu, R.-I., & Wiesen, P. (2020). Secondary organic aerosol formation from nitrophenols photolysis under atmospheric conditions. *Atmosphere*, 11(12), 1346. <https://doi.org/10.3390/atmos11121346>
- Birdsall, A. W., & Elrod, M. J. (2011). Comprehensive NO-dependent study of the products of the oxidation of atmospherically relevant aromatic compounds. *The Journal of Physical Chemistry A*, 115(21), 5397–5407. <https://doi.org/10.1021/jp2010327>
- Brewer, J. F., Jacob, D. J., Jathar, S. H., He, Y., Akherati, A., Zhai, S., et al. (2022). A scheme for representing aromatic secondary organic aerosols in chemical transport models: Application to source attribution of organic aerosols over South Korea during the KORUS-AQ campaign. Retrieved from <https://acmg.seas.harvard.edu/files/acmg/files/brewer2022.pdf>
- Cabrera-Perez, D., Taraborrelli, D., Sander, R., & Pozzer, A. (2016). Global atmospheric budget of simple monocyclic aromatic compounds. *Atmospheric Chemistry and Physics*, 16(11), 6931–6947. <https://doi.org/10.5194/acp-16-6931-2016>
- Carter, W. P. L. (1999). Documentation of the SAPRC-99 chemical mechanism for VOC reactivity assessment volume 1 of 2 documentation text. Coggon, M. M., Gkatzelis, G. I., McDonald, B. C., Gilman, J. B., Schwantes, R. H., Abuhassan, N., et al. (2021). Volatile chemical product emissions enhance ozone and modulate urban chemistry. *Proceedings of the National Academy of Sciences of the United States of America*, 118(32), e2026653118. <https://doi.org/10.1073/pnas.2026653118>
- Crawford, J., Kim, Y., Fried, A., Lefer, B., Jordan, C., Lee, G., et al. (2020). KORUS-AQ final science synthesis report. Retrieved from <https://espo.nasa.gov/sites/default/files/documents/5858211.pdf>
- Crawford, J. H., Ahn, J.-Y., Al-Saadi, J., Chang, L., Emmons, L. K., Kim, J., et al. (2021). The Korea–United States air quality (KORUS-AQ) field study. *Elementa: Science of the Anthropocene*, 9(1). <https://doi.org/10.1525/elementa.2020.00163>
- Eastham, S. D., & Jacob, D. J. (2017). Limits on the ability of global Eulerian models to resolve intercontinental transport of chemical plumes. *Atmospheric Chemistry and Physics*, 17(4), 2543–2553. <https://doi.org/10.5194/acp-17-2543-2017>
- Emmons, L. K., Schwantes, R. H., Orlando, J. J., Tyndall, G., Kinnison, D., Lamarque, J.-F., et al. (2020). The chemistry mechanism in the Community Earth System Model Version 2 (CESM2). *Journal of Advances in Modeling Earth Systems*, 12(4), e2019MS001882. <https://doi.org/10.1029/2019MS001882>
- Fan, J., & Zhang, R. (2006). Atmospheric oxidation mechanism of p-xylene: A density functional theory study. *The Journal of Physical Chemistry A*, 110(24), 7728–7737. <https://doi.org/10.1021/jp061735e>
- Fang, Z., Lai, A., Dongmei, C., Chunlin, L., Carmieli, R., Chen, J., et al. (2024). Secondary organic aerosol generated from biomass burning emitted phenolic compounds: Oxidative potential, reactive oxygen species, and cytotoxicity. *Environmental Science & Technology*, 58(19), 8194–8206. <https://doi.org/10.1021/acs.est.3c09903>
- Finewax, Z., de Gouw, J. A., & Ziemann, P. J. (2018). Identification and quantification of 4-nitrocatechol formed from OH and NO<sub>3</sub> radical-initiated reactions of catechol in air in the presence of NO<sub>x</sub>: Implications for secondary organic aerosol formation from biomass burning. *Environmental Science & Technology*, 52(4), 1981–1989. <https://doi.org/10.1021/acs.est.7b05864>

- Forstner, H. J. L., Flagan, R. C., & Seinfeld, J. H. (1997). Secondary organic aerosol from the photooxidation of aromatic hydrocarbons: Molecular composition. *Environmental Science & Technology*, 31(5), 1345–1358. <https://doi.org/10.1021/es9605376>
- Fredrickson, C. D., Palm, B. B., Lee, B. H., Zhang, X., Orlando, J. J., Tyndall, G. S., et al. (2022). Formation and evolution of catechol-derived SOA mass, composition, volatility, and light absorption. *ACS Earth and Space Chemistry*, 6(4), 1067–1079. <https://doi.org/10.1021/acsearthspacechem.2c00007>
- Gkatzelis, G. I., Coggon, M. M., Stockwell, C. E., Hornbrook, R. S., Allen, H., Apel, E. C., et al. (2024). Parameterizations of US wildfire and prescribed fire emission ratios and emission factors based on FIREX-AQ aircraft measurements. *Atmospheric Chemistry and Physics*, 24(2), 929–956. <https://doi.org/10.5194/acp-24-929-2024>
- Guenther, A. B., Jiang, X., Heald, C. L., Sakulyanontvittaya, T., Duhl, T., Emmons, L. K., & Wang, X. (2012). The model of emissions of gases and aerosols from nature version 2.1 (MEGAN2.1): An extended and updated framework for modeling biogenic emissions. *Geoscientific Model Development*, 5(6), 1471–1492. <https://doi.org/10.5194/gmd-5-1471-2012>
- Huang, M., Zhang, W., Hao, L., Wang, Z., Fang, L., Kong, R., et al. (2010). Experimental study of photooxidation products of ethylbenzene. *Journal of Environmental Sciences*, 22(10), 1570–1575. [https://doi.org/10.1016/S1001-0742\(09\)60291-6](https://doi.org/10.1016/S1001-0742(09)60291-6)
- Koppmann, R. (2007). *Volatile organic compounds in the atmosphere*. John Wiley & Sons. Retrieved from <http://ebookcentral.proquest.com/lib/uow/detail.action?docID=351656>
- Koss, A. R., Sekimoto, K., Gilman, J. B., Selimovic, V., Coggon, M. M., Zarzana, K. J., et al. (2018). Non-methane organic gas emissions from biomass burning: Identification, quantification, and emission factors from PTR-ToF during the FIREX 2016 laboratory experiment. *Atmospheric Chemistry and Physics*, 18(5), 3299–3319. <https://doi.org/10.5194/acp-18-3299-2018>
- Kroftlić, A., Grilc, M., & Grgić, I. (2015). Does toxicity of aromatic pollutants increase under remote atmospheric conditions? *Scientific Reports*, 5(1), 8859. <https://doi.org/10.1038/srep08859>
- Li, M., Zhang, Q., Zheng, B., Tong, D., Lei, Y., Liu, F., et al. (2019). Persistent growth of anthropogenic non-methane volatile organic compound (NMVOC) emissions in China during 1990–2017: Drivers, speciation and ozone formation potential. *Atmospheric Chemistry and Physics*, 19(13), 8897–8913. <https://doi.org/10.5194/acp-19-8897-2019>
- MacFarlane, S. (2025). smm997/KORUS-AQ-Updated-Simulation-Files: KORUS-AQ-Updated-Simulation-Files [Dataset]. *Zenodo*. <https://doi.org/10.5281/zenodo.15320686>
- Majdi, M., Sartelet, K., Lanzafame, G. M., Couvidat, F., Kim, Y., Chrit, M., & Turquet, S. (2019). Precursors and formation of secondary organic aerosols from wildfires in the Euro-Mediterranean region. *Atmospheric Chemistry and Physics*, 19(8), 5543–5569. <https://doi.org/10.5194/acp-19-5543-2019>
- McDonald, B. C., de Gouw, J. A., Gilman, J. B., Jathar, S. H., Akherati, A., Cappa, C. D., et al. (2018). Volatile chemical products emerging as largest petrochemical source of urban organic emissions. *Science*, 359(6377), 760–764. <https://doi.org/10.1126/science.aag0524>
- Mellouki, A., Ammann, M., Cox, R. A., Crowley, J. N., Herrmann, H., Jenkin, M. E., et al. (2021). Evaluated kinetic and photochemical data for atmospheric chemistry: Volume VIII – Gas-phase reactions of organic species with four, or more, carbon atoms ( $\geq C_4$ ). *Atmospheric Chemistry and Physics*, 21(6), 4797–4808. <https://doi.org/10.5194/acp-21-4797-2021>
- Miao, R., Chen, Q., Zheng, Y., Cheng, X., Sun, Y., Palmer, P. I., et al. (2020). Model bias in simulating major chemical components of PM<sub>2.5</sub> in China. *Atmospheric Chemistry and Physics*, 20(20), 12265–12284. <https://doi.org/10.5194/acp-20-12265-2020>
- NASA. (2016). KORUS-AQ flight summaries. Retrieved from [https://www-air.larc.nasa.gov/missions/korus-aq/docs/KORUS-AQ\\_Flight\\_Summaries\\_ID122.pdf](https://www-air.larc.nasa.gov/missions/korus-aq/docs/KORUS-AQ_Flight_Summaries_ID122.pdf)
- NASA. (2025). Korea United States air quality study [Dataset]. *NASA*. <https://doi.org/10.5067/Suborbital/KORUSAQ/DATA01>
- Noda, J., Volkamer, R., & Molina, M. J. (2009). Dealkylation of alkylbenzenes: A significant pathway in the toluene, o-m-p-xylene + OH reaction. *The Journal of Physical Chemistry A*, 113(35), 9658–9666. <https://doi.org/10.1021/jp901529k>
- Peng, Y., Yuan, B., Yang, S., Wang, S., Yang, X., Wang, W., et al. (2023). Photolysis frequency of nitrophenols derived from ambient measurements. *Science of the Total Environment*, 869, 161810. <https://doi.org/10.1016/j.scitotenv.2023.161810>
- Perrone, M. G., Carbone, C., Faedo, D., Ferrero, L., Maggioni, A., Sangiorgi, G., & Bolzacchini, E. (2014). Exhaust emissions of polycyclic aromatic hydrocarbons, n-alkanes and phenols from vehicles coming within different European classes. *Atmospheric Environment*, 82, 391–400. <https://doi.org/10.1016/j.atmosenv.2013.10.040>
- Rajabi, H., Hadi Mosleh, M., Mandal, P., Lea-Langton, A., & Sedighi, M. (2020). Emissions of volatile organic compounds from crude oil processing – Global emission inventory and environmental release. *Science of the Total Environment*, 727, 138654. <https://doi.org/10.1016/j.scitotenv.2020.138654>
- Schwantes, R. H., Lacey, F. G., Tilmes, S., Emmons, L. K., Lauritzen, P. H., Walters, S., et al. (2022). Evaluating the impact of chemical complexity and horizontal resolution on tropospheric ozone over the conterminous US with a global variable resolution chemistry model. *Journal of Advances in Modeling Earth Systems*, 14(6), e2021MS002889. <https://doi.org/10.1029/2021MS002889>
- Seinfeld, J. H., & Pandis, S. N. (2016). *Atmospheric chemistry and physics: From air pollution to climate change*. John Wiley & Sons. Retrieved from <http://ebookcentral.proquest.com/lib/uow/detail.action?docID=4462549>
- Shuai, J., Kim, S., Ryu, H., Park, J., Lee, C. K., Kim, G.-B., et al. (2018). Health risk assessment of volatile organic compounds exposure near Daegu dyeing industrial complex in South Korea. *BMC Public Health*, 18(1), 528. <https://doi.org/10.1186/s12889-018-5454-1>
- Simpson, I. J., Blake, D. R., Blake, N. J., Meinardi, S., Barletta, B., Hughes, S. C., et al. (2020). Characterization, sources and reactivity of volatile organic compounds (VOCs) in Seoul and surrounding regions during KORUS-AQ. *Elementa: Science of the Anthropocene*, 8. <https://doi.org/10.1525/elementa.434>
- Song, K., Guo, S., Wang, H., Yu, Y., Wang, H., Tang, R., et al. (2021). Measurement report: Online measurement of gas-phase nitrated phenols utilizing a CI-LToF-MS: Primary sources and secondary formation. *Atmospheric Chemistry and Physics*, 21(10), 7917–7932. <https://doi.org/10.5194/acp-21-7917-2021>
- Stanevich, I., Jones, D. B. A., Strong, K., Parker, R. J., Boesch, H., Wunch, D., et al. (2020). Characterizing model errors in chemical transport modeling of methane: Impact of model resolution in versions v9-02 of GEOS-Chem and v35j of its adjoint model. *Geoscientific Model Development*, 13(9), 3839–3862. <https://doi.org/10.5194/gmd-13-3839-2020>
- The International GEOS-Chem User Community. (2022). geoschem/GCClassic: GEOS-Chem 13.4.0 (Version 13.4.0) [Software]. *Zenodo*. <https://doi.org/10.5281/zenodo.6511970>
- Tiwari, J., Tarale, P., Sivanesan, S., & Bafana, A. (2019). Environmental persistence, hazard, and mitigation challenges of nitroaromatic compounds. *Environmental Science and Pollution Research*, 26(28), 28650–28667. <https://doi.org/10.1007/s11356-019-06043-8>
- Travis, K. R., Nault, B. A., Crawford, J. H., Bates, K. H., Blake, D. R., Cohen, R. C., et al. (2024). Impact of improved representation of volatile organic compound emissions and production of NO<sub>x</sub> reservoirs on modeled urban ozone production. *Atmospheric Chemistry and Physics*, 24(16), 9555–9572. <https://doi.org/10.5194/acp-24-9555-2024>

- Wainwright, C. D., Pierce, J. R., Liggio, J., Strawbridge, K. B., Macdonald, A. M., & Leitch, R. W. (2012). The effect of model spatial resolution on secondary organic aerosol predictions: A case study at Whistler, BC, Canada. *Atmospheric Chemistry and Physics*, 12(22), 10911–10923. <https://doi.org/10.5194/acp-12-10911-2012>
- Wang, L., Wu, R., & Xu, C. (2013). Atmospheric oxidation mechanism of benzene. Fates of alkoxy radical intermediates and revised mechanism. *The Journal of Physical Chemistry A*, 117(51), 14163–14168. <https://doi.org/10.1021/jp4101762>
- Woo, J.-H., Kim, Y., Kim, H.-K., Choi, K.-C., Eum, J.-H., Lee, J.-B., et al. (2020). Development of the CREATE inventory in support of integrated climate and air quality modeling for Asia. *Sustainability*, 12(19), 7930. <https://doi.org/10.3390/su12197930>
- Xu, L., Crounse, J. D., Vasquez, K. T., Allen, H., Wennberg, P. O., Bourgeois, I., et al. (2021). Ozone chemistry in western U.S. wildfire plumes. *Science Advances*, 7(50), eabl3648. <https://doi.org/10.1126/sciadv.abl3648>
- Xu, L., Möller, K. H., Crounse, J. D., Kjaergaard, H. G., & Wennberg, P. O. (2020). New insights into the radical chemistry and product distribution in the OH-initiated oxidation of benzene. *Environmental Science & Technology*, 54(21), 13467–13477. <https://doi.org/10.1021/acs.est.0c04780>
- Yan, Y., Cabrera-Perez, D., Lin, J., Pozzer, A., Hu, L., Millet, D. B., et al. (2019). Global tropospheric effects of aromatic chemistry with the SAPRC-11 mechanism implemented in GEOS-Chem version 9-02. *Geoscientific Model Development*, 12(1), 111–130. <https://doi.org/10.5194/gmd-12-111-2019>
- Yu, K., Jacob, D. J., Fisher, J. A., Kim, P. S., Marais, E. A., Miller, C. C., et al. (2016). Sensitivity to grid resolution in the ability of a chemical transport model to simulate observed oxidant chemistry under high-isoprene conditions. *Atmospheric Chemistry and Physics*, 16(7), 4369–4378. <https://doi.org/10.5194/acp-16-4369-2016>
- Yuan, B., Liggio, J., Wentzell, J., Li, S. M., Stark, H., Roberts, J. M., et al. (2016). Secondary formation of nitrated phenols: Insights from observations during the Uintah Basin winter ozone study (UBWOS) 2014. *Atmospheric Chemistry and Physics*, 16(4), 2139–2153. <https://doi.org/10.5194/acp-16-2139-2016>
- Zeng, P., Guo, H., Cheng, H., Wang, Z., Zeng, L., Lyu, X., et al. (2019). Aromatic hydrocarbons in urban and suburban atmospheres in central China: Spatiotemporal patterns, source implications, and health risk assessment. *Atmosphere*, 10(10), 565. <https://doi.org/10.3390/atmos10100565>
- Zheng, B., Tong, D., Li, M., Liu, F., Hong, C., Geng, G., et al. (2018). Trends in China's anthropogenic emissions since 2010 as the consequence of clean air actions. *Atmospheric Chemistry and Physics*, 18(19), 14095–14111. <https://doi.org/10.5194/acp-18-14095-2018>